PSFC/RR-07-2

Magnetic Forces of Electromagnetic Bougienage

Makoto Takayasu, D. Bruce Montgomery*, and
Joseph V. Minervini

September 2008

Plasma Science and Fusion Center
Massachusetts Institute of Technology
Cambridge MA 02139 USA

*** Magplane Technology, Inc.**
380 Hanscom drive
Bedford, MA 01730

This work was supported by the U.S. National Institute of Health and Children's Hospital Charitable Funds, Boston.

Abstract

An electromagnetic bougienage method to lengthen esophageal segments of infants born with esophageal-atresia was developed thirty years ago by Hendren and Hale. In this treatment magnetic material bougie bullets were placed in the two ends of the esophagus. A magnetic field applied across the infant's chest was used to attract the bougies to stretch the esophageal tissue. When the two esophageal segments were sufficiently close after one to two months of treatment, they could be surgically joined together. This approach has been performed successfully and confirmed to be feasible for infants whose esophageal separations are too wide for direct surgical repair. However, the technique was not further developed at that time. Recently Magplane Technology, Inc. has developed a next generation device for electromagnetic bougienage that meets modern hospital standards for safety and ease of use. In this report we present characteristics of a prototype bougienage magnet system that has been fabricated and tested. Two types of bullets, solid rounded rod bullet and hollow cylinder bullet for an electromagnetic bougienage have been developed. Measurements of magnetic forces acting on bougie bullets in the magnet field have been discussed along with calculation results of analytical methods developed to obtain the magnetic forces on the bougie. The calculation results were confirmed to agree with the experimental results. The analytical equations obtained can be used for an active bougienage force control system while in use during hospital operation.

Contents

1. Introduction

2. Magnet and Magnetic Force Measurement Setup

- 2.1 Magnet Winding Dimensions
- 2.2 Magnet Specification

3. Magnet Operation

- 3.1 Magnet Operation Temperature
- 3.2 Magnet Field and Field Distribution along the magnet axis
- 3.3 Calculated Magnetic Field

4. Bougie Bullets and Magnetization

5. Magnetic Force Measurements

- 5.1 Force for two bullets
  - 5.1.1 Two Rounded Rod Bullets
  - 5.1.2 Two Hollow Cylinder Bullets
- 5.2 Force for one bullet
- 5.3 Off-centered two-bullet force
- 5.4 Radial force
  - 5.4.1 Two-bullet radial force
  - 5.4.2 One-bullet radial force

6. Magnetic Force and Field Analyses

- 6.1 Magnetic Force and Field Analysis Methods
- 6.2 Analytical Force Equations
  - 6.2.1 Rounded rod bullet
  - 6.2.2 Hollow cylinder bullet
- 6.3 Calculation Results
  - 6.3.1 Two Bullet Force
  - 6.3.2 One Bullet Force
  - 6.3.3 Off-Centered Two-Bullet Force

7. Pressure Monitoring Method

8. Summary

Acknowledgements

References

1. Introduction

The esophagus in esophageal atresia fails to bridge the connection from the mouth to the stomach. Over the past half century esophageal atresia has been treated by primary anastomoses, colon or gastric tube interposition graft, manual bougienage, or by electromagnetic bougienage. When the two esophageal segments are sufficiently close, they can be joined by anastomosis without tension (90% of cases). However, for approximately 100 babies/yr in the United States (7.5% of cases), the two ends of the esophagus are too widely separated for this remedy.

For these cases, the most common procedure is to interpose a segment of colon to bridge the distance. This is an extremely arduous procedure for the infant. As an alternative to the use of colonic graft, Howard and Myers [1] introduced mechanical bougienage into the lumen of the upper esophageal segment. They used a regimen of daily manual stretching of the esophageal tissue over a 30-day period. This alternating application of a tissue stretching force followed by relaxation promoted tissue growth to the point where surgery could be successfully performed.

An electromagnetic bougienage method to lengthen the esophageal segments using a magnetic force was developed in 1975 by Hendren and Hale [2], [3]. Magnetic bougie bullets were placed in the two ends of the esophagus. An electromagnetic field was applied across the infant's chest to attract the bougies, in order to stretch the esophageal tissue for one minute, followed by one minute of relaxation, with the cycle typically repeated. When the two esophageal segments were sufficiently close after one to two months of treatment, they could be surgically jointed together. In the four trial cases the ends of the esophagus were seen to become elongated and thickened allowing successful primary repair. Hendren and Hale also applied the electromagnetic bougienage for a surgical repair of an imperforate anus, four cases of which were also treated using the electromagnetic bougienage in 1976 [4]. The occurrence of imperforate anus is approximately 1 in 5000 births, approximately half as frequent as that of esophageal atresia. The electromagnetic bougienage technique was not further developed at that time since the use of the magnetic method was not welcome to a hospital.

Recently an application of the electromagnetic bougienage has been reported to attempt primary repair of short gap esophageal atresia without major surgical intervention by Zaritsky of Children's Hospital, La Plata, Argentina [5]. Permanent magnets were inserted into each pouch and used to force anastomoses of the pouches. The resulting problematic esophageal stenosis was then approached by the use of balloon dilations.

Magplane Technology, Inc. recently has developed a next generation device for electromagnetic bougienage that meets modern hospital standards for safety and ease of use and which will utilize recent technological advances. It should be noted that the new basic crib structure makes it very easy for the nurse to reach in and pick up the baby at any time for care and interactions.

In this report we present characteristics of a prototype bougienage magnet that has been fabricated and tested. The bougie magnet was operated with the full current of 800 A.

The tests include the operation of the magnet, measurements of magnetic forces acting on two types of bougie bullets; rounded rod bullets and hollow cylinder bullets. Characteristics of magnetic bullet forces were presented along with discussion of analytical method developed for calculating the forces on the bougie. To monitor the pressure of the bullet acting on tissue during treatments, the magnetic forces a wireless bullet-pressure measurement method has been proposed using SmartPill® of the SmartPill Co. and preliminarily tested.

2. Magnet and Magnetic Force Measurement Setup

2.1 Magnet Winding Dimensions

The magnet is composed of six elliptical racetrack double pancakes with eight layers of a hollow conductor (0.354" square O.D. and 0.177" I.D.). The magnet has a bore of the major diameter of 13.02" (330.6 mm) and the minor diameter of 9.39" (238.6 mm), and the height of 4.52" (114.8 mm), which were designed to fit the infant's chest.

Table 2.1 Major and minor radii of the winding turns of the magnet.

Winding Turns	Major Radius a (mm)	Minor Radius b (mm)
Inner edge	165.3	119.3
1st	169.9	123.9
2nd	179.2	133.2
3rd	188.41	142.4
4th	197.6	151.6
5th	206.9	160.9
6th	216.1	170.1
7th	225.3	179.3
8th	234.6	188.6
Outer edge	239.2	193.2

Table 2.2 Layer height of the winding turns of the magnet.

Layer	z (mm)
Top edge	57.4
1st	52.6
2nd	43.1
3rd	33.5
4th	23.9
5th	14.4
6th	4.8
7th	-4.8
8th	-14.4
9th	-23.9
10th	-33.5
11th	-43.1
12th	-52.6
Bottom edge	-57.4

The magnet was designed by Robert Weggel and fabricated by Stonite Coil Corporation. Fig. 2.1 shows the magnet with a bullet force measurement set up described later. Measured dimensions of the winding turns and the layers of the fabricated magnet are given from the magnet center in Tables 2.1. and 2.2. The dimensions are given by the centerline of the conductor, unless otherwise stated.

2.2 Magnet Specification

Electrical specifications of the magnet are:

Resistance	32.3 m-Ohm
Inductance measured	2.7 mH
Maximum current	800 A with proper cooling
Voltage	26 V
Maximum power	20.7 kW

3. Magnet Operation

3.1 Magnet Operation Temperature

Fig 3.1 shows the inlet and outlet temperatures with the magnetic field for a full current charge of 800 A. The magnet was cooled by a cooling system used for various experiments in our Lab. The flow rate was about 2.2 G/min which was less than the design value of 3 G/min. The temperatures were measured with thermistor temperature sensors. The center field on the axis was 2.72 k-Oe at 800 A. For the 800 A operation the outlet temperature increased in 8 minuets by about 36 °C. When the current was turned off, the outlet temperature decreased sharply. In Fig. 3.1, the temperatures of both the inlet and outlet were gradually increasing for about 500 seconds. It was due to the returned warmed coolant of the cooling system. The temperature seemed to be almost the saturation value. The magnet operations at 500 A, 566 A, 600 A and 700 A for 15 minuets are shown with the 800 A operation of 8 minuets in Fig. 3.2. The temperature increases is plotted as a function of square of I^2 in Fig. 3.3. It was found that the magnet temperature rise ΔT is given by

$$\Delta T = 5.6960 \cdot 10^{-5} \cdot I^2 \qquad (3.1)$$

here I is in ampere.
The temperature increase at 566 A was about 19 °C. It means that 50% duty cycle operation at the full current of 800 A will result the 19 °C temperature rise.

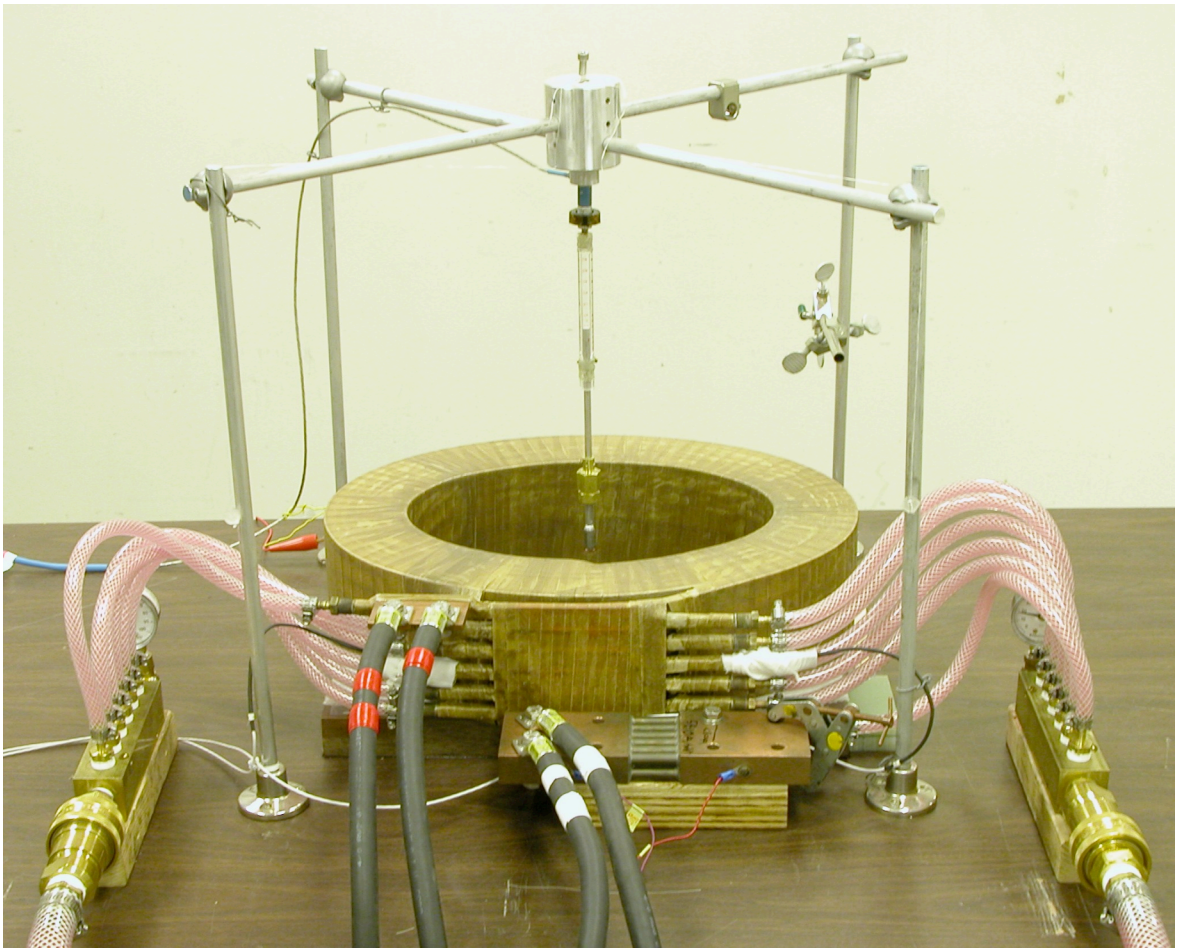

(a)

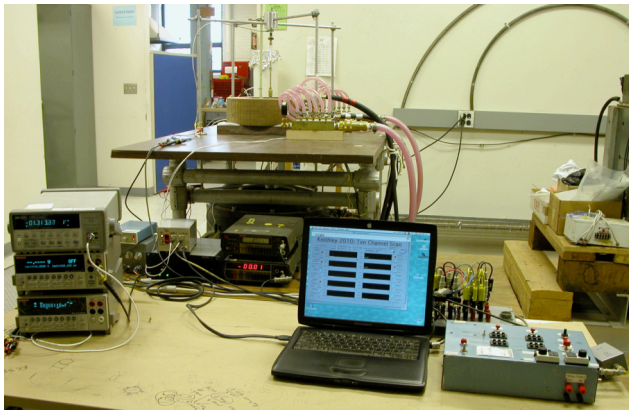

(b)

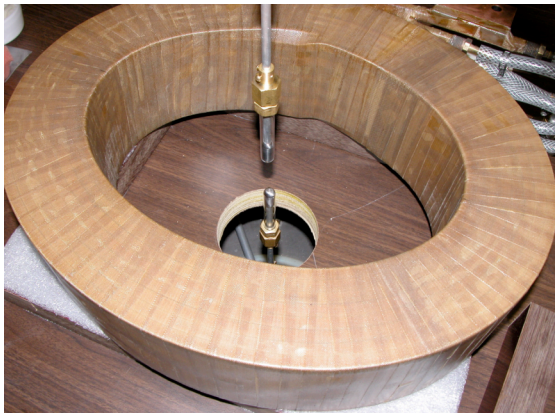

(c)

Fig. 2.1 (a) Magnet with a bullet force measurement setup; one bullet suspended on a load cell at the top. (b) Magnet test setup with a data acquisition system. (c) Two bullets are placed on the magnet axis. The lower bullet is mounted under the magnet.

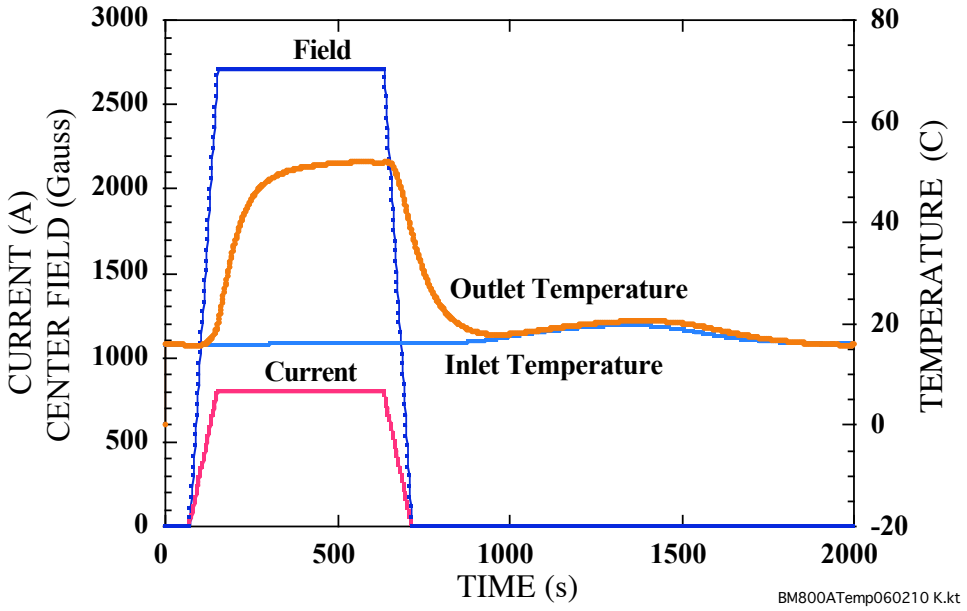

Fig. 3.1 The current, the field at the magnet center, and the inlet and outlet temperatures as a function of time for the full current operation of 800 A for 8 minuets.

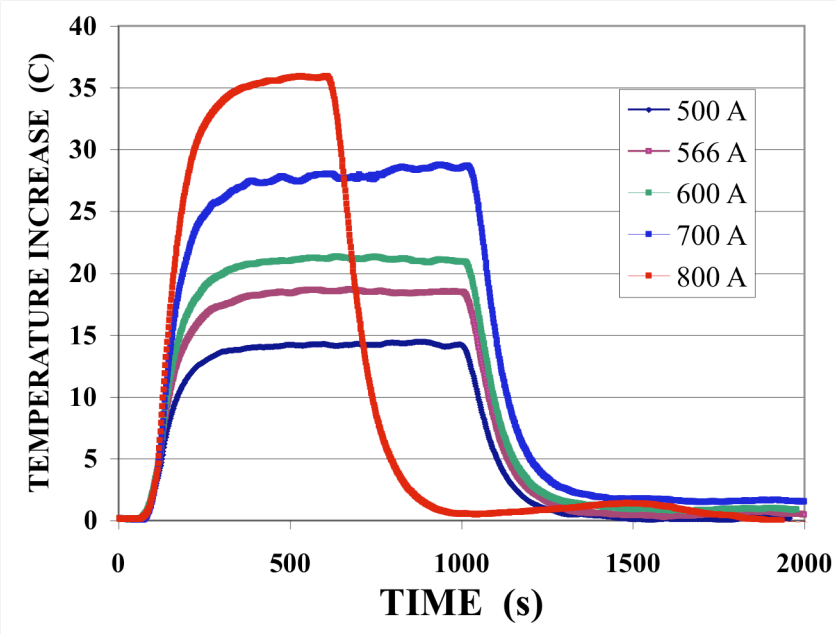

Fig. 3.2 Measured magnet temperature increases at various currents as a function of time for continuous 15 minuets operations at 500 A, 566 A, 600 A and 700 A with an 8 min. operation at 800 A.

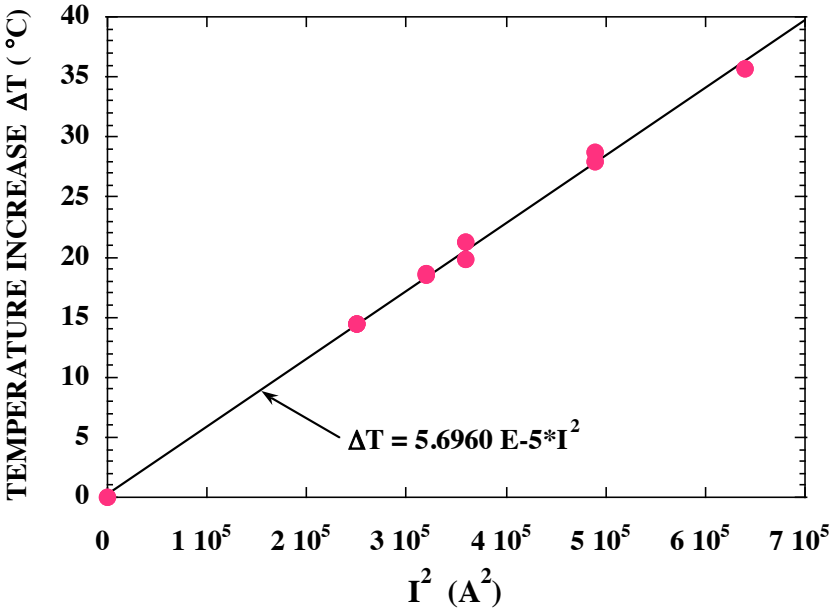

Fig. 3.3 Linear relation between measured magnet temperature increase ΔT and I^2.

3.2 Magnet Field and Field Distribution along the magnet axis

The center field on the magnet axis was measured by calibrated Hall sensor (HGT-3030/3888). The field H is given by

$$H = 3.3984 \cdot I \qquad (3.2)$$

here H is in Oe, and I is the current in A.

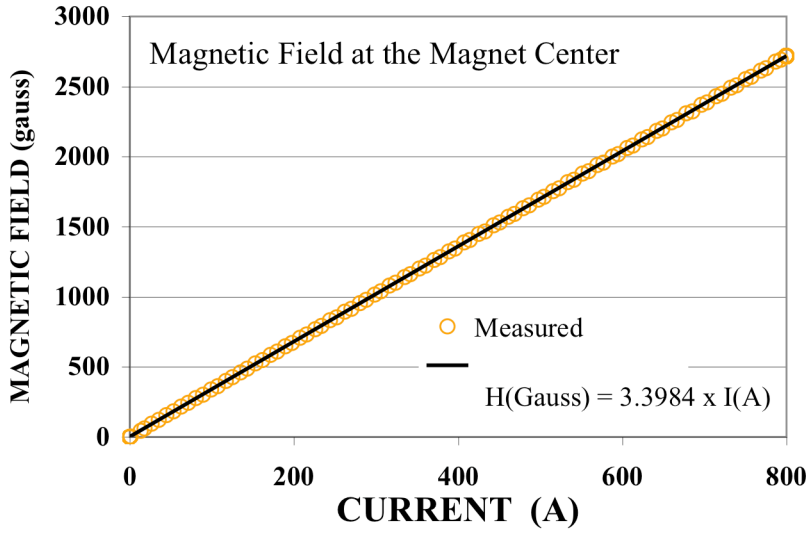

Fig. 3.4 Magnetic field at the center vs. the current. The solid line is the fitted line.

3.3 Calculated Magnetic Field

The coil winding shape was an elliptical-shaped racetrack, not exactly elliptic. However, each winding was approximated by an elliptical single turn coil of the major diameter ξ and the minor diameter η to calculate the magnetic field and the field distribution on the magnet axis. The center field H on the axis of the elliptical coil is given at the current I by,

$$H = \frac{E(\varepsilon)}{\pi\xi} I \qquad (3.3)$$

where

$$E(\varepsilon) = \int_0^{\pi/2} \sqrt{1 - \varepsilon^2 \cdot \sin^2 \varphi} \cdot d\varphi \quad \text{(The Elliptic Integral of the second kind)}$$

$$\varepsilon = \sqrt{\frac{\xi^2 - \eta^2}{\xi^2}} \qquad (3.4)$$

To calculate the field along the magnet axis, an equivalent circular coil to the elliptical coil having the same center field is used. The radius of such equivalent circular coil is

$$\delta = \frac{I}{2H} \qquad (3.5)$$

The axial field H(x) of the circular coil is given as a function of the distance x from the magnet center [6];

$$H(x) = \frac{\delta^2 I}{2(\delta^2 + x^2)^{3/2}} \qquad (3.6)$$

The total field of the magnet composed of the six double pancake and eight layers was obtained by a summation of the fields of 96 coils using Eq. (3.6) for each coil. The calculated field H(Oe) along the axis is well approximated with the following equation for x = 0 to 100 mm;

$$H = (2.0885\text{x}10^{-9}\ \text{x}^4 + 1.8797\text{x}10^{-7}\ \text{x}^3 - 1.4406\text{x}10^{-4}\ \text{x}^2 + 6.4422\text{x}10^{-5}\ \text{x} + 3.3060)\ I \qquad (3.7)$$

where x is in mm.

Fig 3.5 shows the calculated field along the magnet axis. In Fig. 3.5(b) the results were compared with the measured value at the magnet current of 200 A. It shows that the calculated field was 2.72% smaller than the measured value. Note that the following field and force calculations discussed here are not corrected with this error of 2.72%.

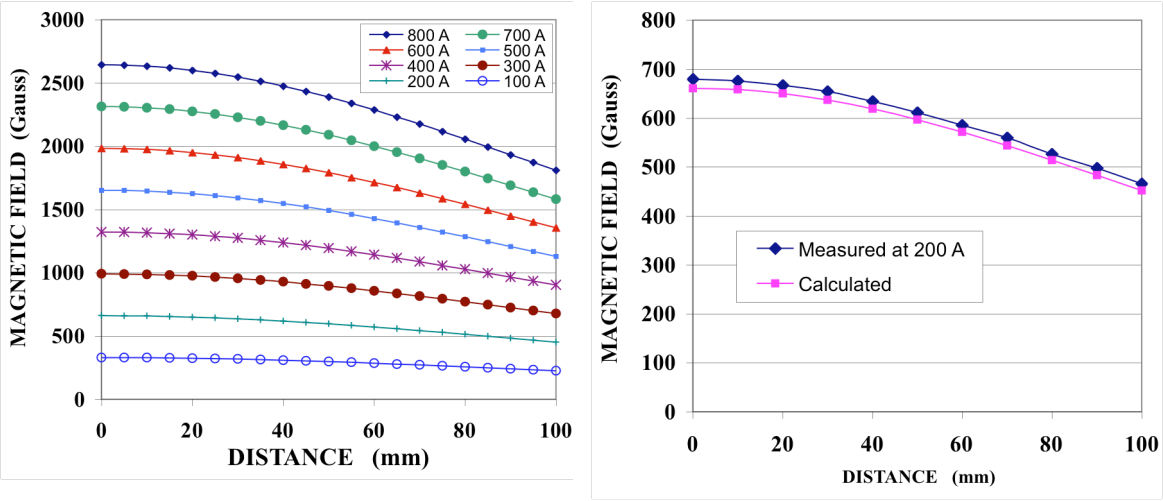

(a) (b)

Fig 3.5 Magnetic field along the magnet axis. (a) Calculated fields at various operation currents. (b) The calculated field is compared with the measured value at the current of 200 A.

4. Bougie Bullets and Magnetization

Three types of bougie bullets were fabricated as shown in Fig. 4.1. The bullets were made of magnetic stainless steel 420, except Bullet C of stainless steel 430 wires are

A. Rounded rod bullet: 25 mm long, 10 mm diameter rounded rod bullet (Each end is a half sphere of 10 mm diameter), weight 13.2 g.

B. Hollow cylinder bullet : 25 mm long, 10 mm OD, 7 mm ID cylinder, weight 7.9 g.

C. Wire assembly bullet: Assembly of 17 wires (Wire: 25 mm long, 1 mm Diameter SS 430), weight 2.7 g.

Fig. 4.1 Bullets from left:
A. Rounded rod bullet (13.2 g)
B. Hollow cylinder bullet (7.9 g)
C. Wire assembly bullet (2.7 g)

Bullet magnetizations were evaluated by measuring magnetic fields of the bullets using a Hall sensor in homogenous field. Fig. 4.2 (a) shows the magnetizations of these three bullets. The saturation magnetization was fixed at 1.7 T of the handbook value. The magnetization of the hollow cylinder bullet saturates at lower field than that of the rounded rod bullet since the hollow cylinder has less demagnetization field effect than the

rod. Estimated magnetic moments of the rounded rod and cylinder bullets are shown in Fig. 4.2 (b). The cylinder bullet has almost a half of the magnetic moment of the rod bullet since the volume of the cylinder bullet is almost a half of that of the rod bullet.

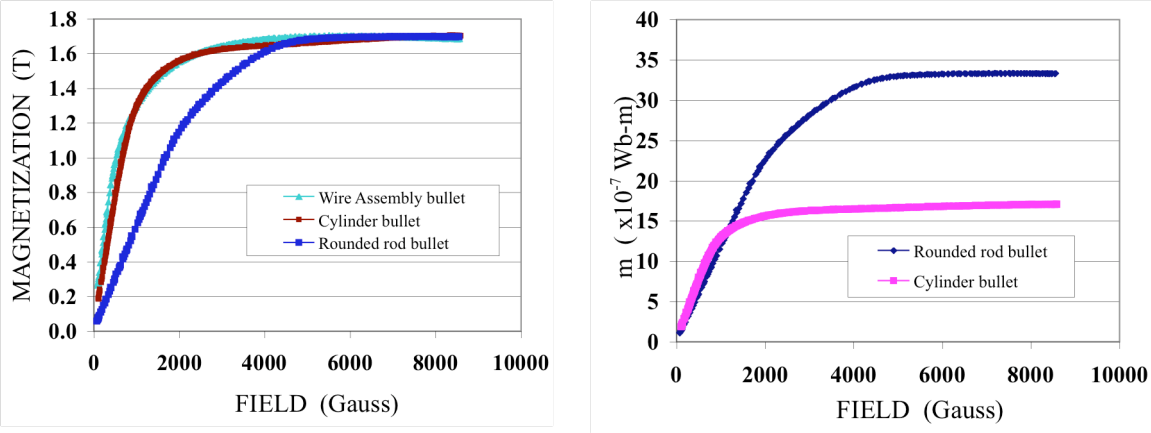

(a) (b)

Fig. 4.2 Magnetization vs. field curves of various bougie bullets shown in the previous figure. (a) Measured magnetization curves using the saturation magnetization 1.7 T, (b) Estimated magnetic moments of the rounded rod and cylinder bullets.

The measured magnetization curves shown in Fig. 4.2 (a) were approximated by the following equations:

Rounded rod bullet:

$$J_m(H) = -2.3986\ 10^{-19} H^5 + 5.270810^{-15} H^4 - 3.5226\ 10^{-11} H^3 + 1.474610^{-8} H^2 + 6.3306\ 10^{-4} H + 2.7062\ 10^{-3} \quad (4.1)$$

Hollow cylinder bullet:

$$J_m(H) = -1.4105\ 10^{-22} H^6 + 4.4854\ 10^{-18} H^5 - 5.7173\ 10^{-14} H^4 + 3.7226\ 10^{-10} H^3 - 1.3024\ 10^{-6} H^2 + 2.3417\ 10^{-3} H - 9.1580\ 10^{-2} \quad (4.2)$$

here $J_m(H)$ is in tesla, and H is in Oe. These equations were used for the following force and field calculations.

The magnetization of the hollow cylinder bullet saturates at lower field than that of the rounded rod bullet since the hollow cylinder has less demagnetization field effect than the rod. The cylinder bullet has about half of the saturated magnetic moment as the rod bullet since the volume of the cylinder bullet is about half that of the rod bullet.

5. Magnetic Force Measurements

5.1 Force for two bullets

Two bullets (Upper and Lower bullets) were placed on the magnet axis as illustrated in Fig.5.1. The center between two bullets (S=2 z_a) was at the magnet center plane. The lower bullet was fixed on a supporting holder. The upper bullet was suspended on a load cell (LCFA-1KG), as shown earlier in Fig. 2.1. Magnetic forces on the bullets were measured as a function of the applied magnetic field while changing the separations S between the bullets. Two pairs of different types of bullets, rounded rod bullets and cylinder bullets shown in Fig. 4.1, were used for the following force measurements.

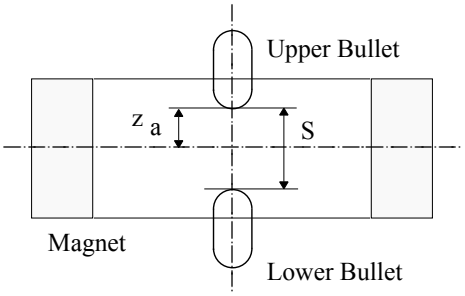

Fig. 5.1 Illustration of the arrangement of two bullets and the magnet.

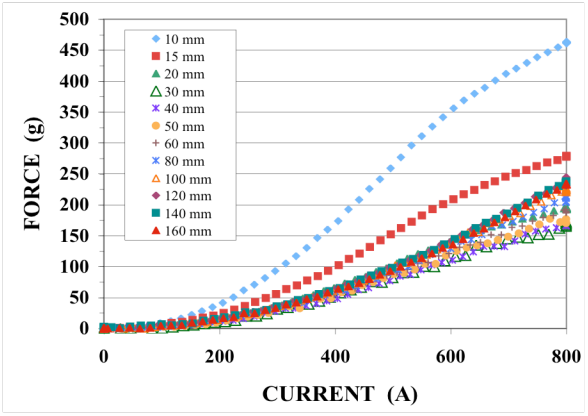

(a)

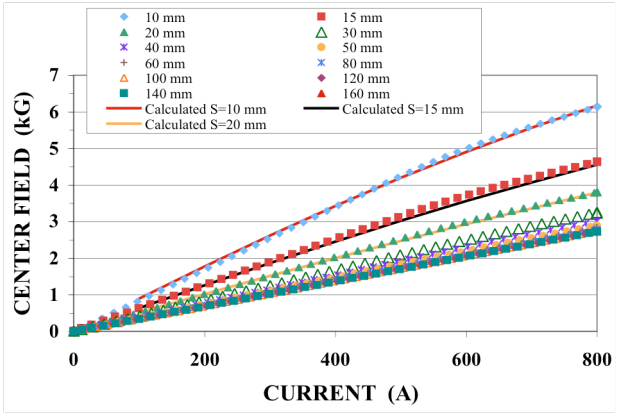

(b)

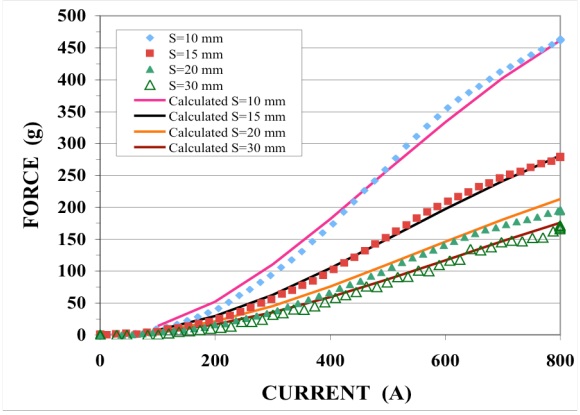

(c)

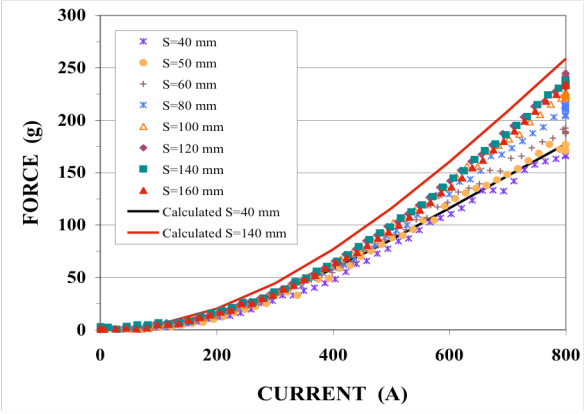

(d)

Fig. 5.2 Measured magnetic force for two rounded rod bullets (a), (c) and (d). Two bullets were placed on the magnet axis and the magnet center plane was at the center of two bullets. The magnetic field measured at the magnet center (b). The solid lines in (c) and (d) are calculated.

5.1.1 Two Rounded Rod Bullets

Fig. 5.2 shows magnetic force between the rounded rod bullets measured as a function of the magnet current for various separation distances between two bullets placed on the magnet axis. The magnet center plain was the center of two bullets. The separation of the bullets was changed from 10 mm to 160 mm. The maximum force was 462 g at 10 mm separation and at a current of 800 A. The forces decrease sharply with increasing the separation up to 30 mm, and then the forces increase gradually with increasing separation. To show this behavior more clearly Fig. 5.2 (a) are separated into Figs. 5.2 (c) and (d). Fig. 5.2 (b) shows the field measured at the magnet center on the magnet axis. The solid lines in these figures show the calculated forces which are discussed later.

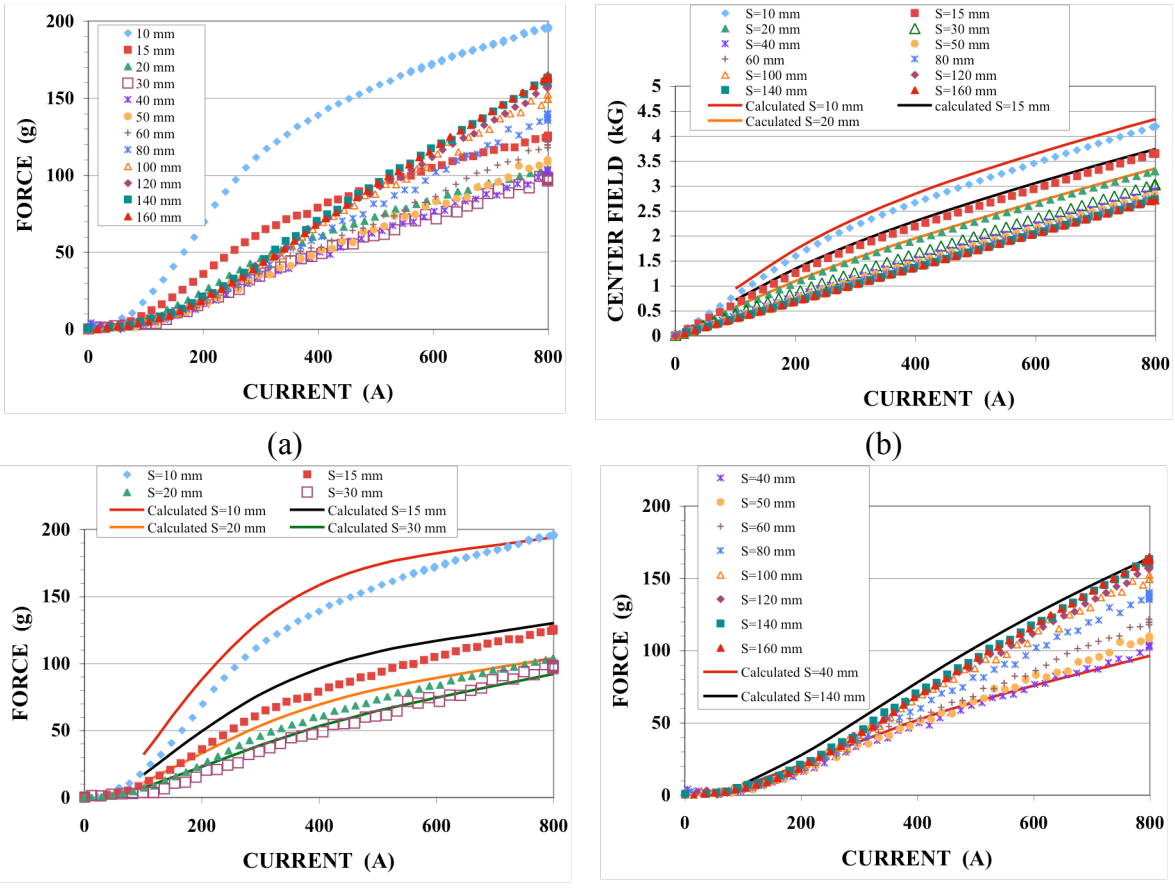

Fig. 5.3 Measured magnetic force for two cylinder bullets. Two bullets were placed on the magnet axis and the magnet plane was at the center of two bullets (a), (c) and (d). The magnetic field measured at the magnet center (b).

5.1.2 Two Hollow Cylinder Bullets

Magnetic force and field data for two cylinder bullets are shown in Fig. 5.3. Compared with the force of the round rod bullet, the magnetic force is smaller for the cylinder bullet in the higher current region since the volume of the cylinder bullet is only about half that of the rod bullet. However, it is noted that the cylinder bullet has larger force at lower current (lower field) even if the volume is smaller, since the cylinder bullet has less demagnetization effect.

5.2 Force for one bullet

Magnetic force experienced with one bullet on the magnet axis (See Fig. 5.4.) was measured in the same way as that for two bullets. In this case the magnetic force is created by only the magnetic field gradient. Measured magnetic forces for one rounded rod bullet and one cylinder bullet are shown in Figs. 5.5 (a) and (b), respectively. As seen in Fig. 5.5, magnetic force increases with increasing the distance z_a from the magnet center, and the maximum force was observed at about z_a=60 mm.

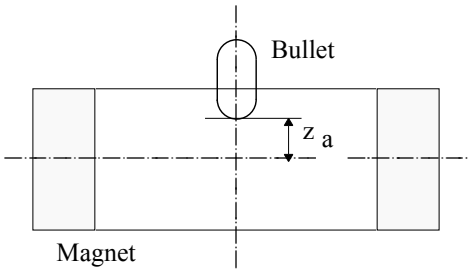

Fig. 5.4 Illustration of the arrangement of one bullet and the magnet.

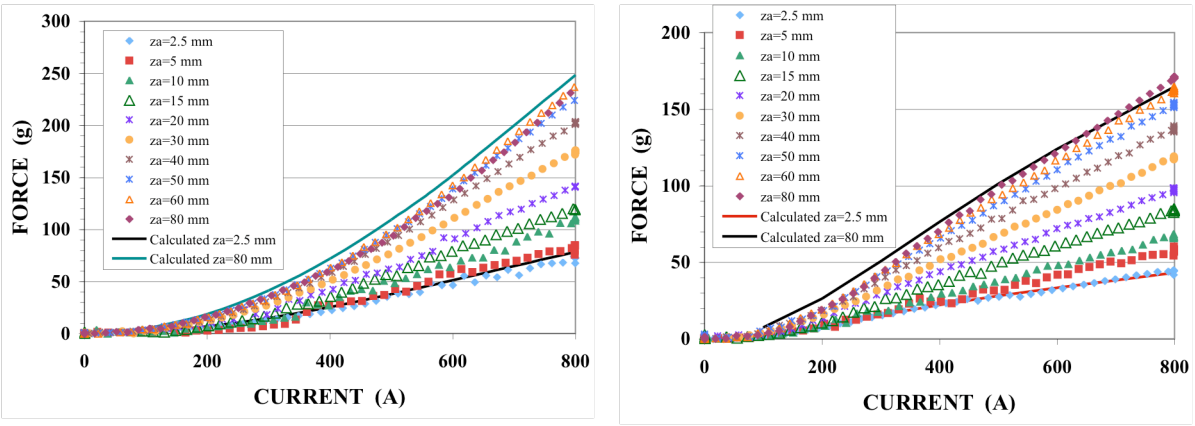

(a) (b)

Fig. 5.5 Measured magnetic force for (a) one rounded rod bullet and (b) one cylinder bullet located at various distances from the magnet center.

5.3 Off-centered two-bullet force

A pair of two bullets was off-centered so that the center between the bullets was not on the magnet center, as shown in Fig. 5.6. The separation of the bullets was kept to be S =

40 mm. Figs. 5.7 (a) and (b) are for the round rod and cylinder bullets, respectively. These figures show the magnetic forces experienced by the upper bullet located at z_a from the magnet center. As seen in Fig. 5.7, the magnetic forces increase with the distance z_a.

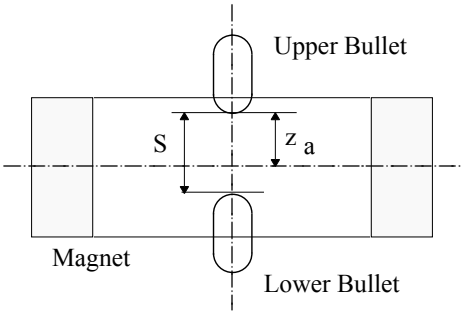

Fig. 5.6 Illustration of the arrangement of off-centered two-bullets and the magnet.

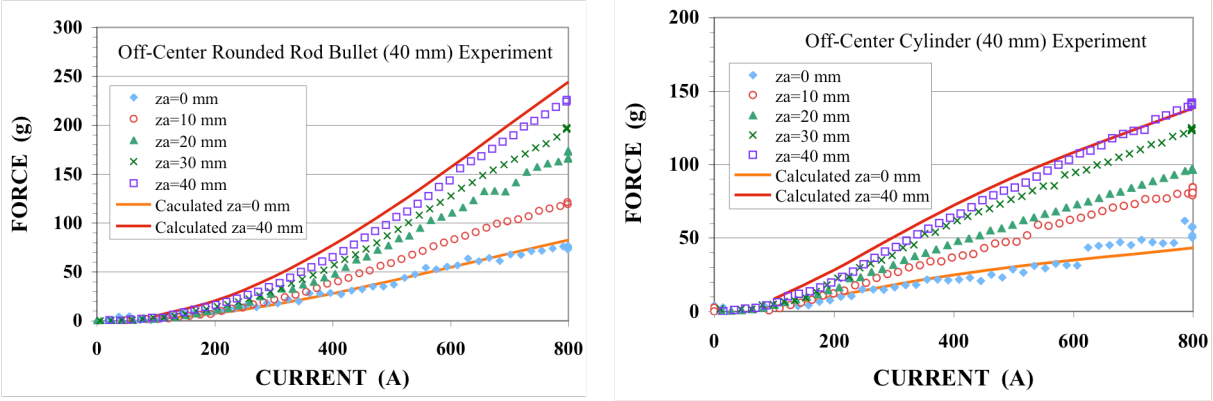

(a) (b)

Fig. 5.7 Measured magnetic force for off-centered two-bullet arrangement. The separation of two bullet was kept to be S=40 mm. (a) The rounded rod bullet. (b) the cylinder bullet.

5.4 Radial force

5.4.1 Two-bullet radial force

The magnetic field creates radial forces as well as the axial force. As seen in Fig. 5.8, a bullet moves toward the magnet winding in a certain condition. In our present force measurement setup the lower bullet was fixed and the upper bullet was movable and measured the magnetic force. The upper bullet was centered by the magnetic mutual force between two bullets. However, if the separation between two bullets increased and their mutual fore reduced, the radial force became dominants and the upper bullet is attracted toward the magnet winding away from the magnet axis by the radial force. It is noted roughly speaking that the bullet is at the outside area of the magnet thickness has the radial force toward the magnet axis and the bullet is automatically centered on the magnet axis.

The radial force was evaluated by a quick method. This method did not provide very accurate data, but it was good enough to see the behavior of the radial force. The radial force was measured using an electric portable balance with a biased weight to measure a pulling force due to the radial force. The bullet was connected to the weight on the balance with a fine string. The setup used is seen in Fig. 5.8 (a).

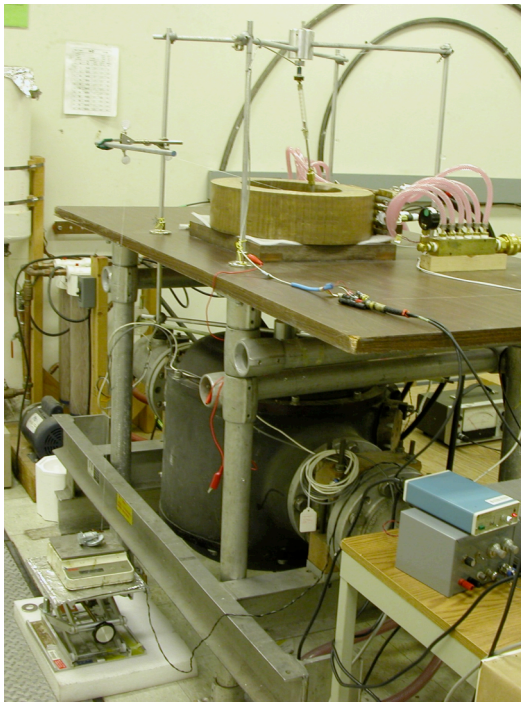

(a)

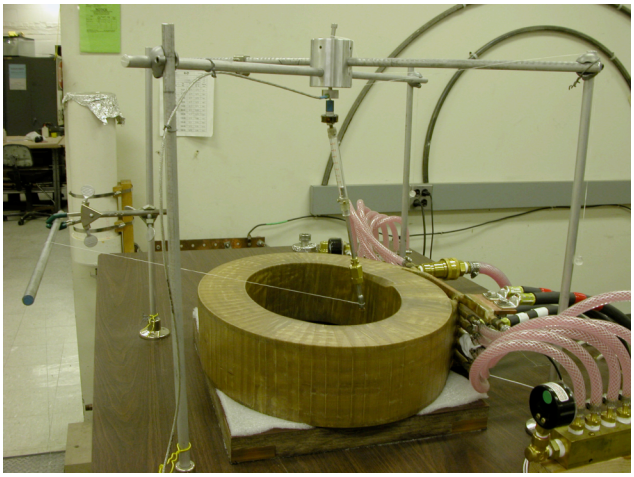

(b)

Fig. 5.8 (a) Demonstrating the radial force on a bullet and the radial force measurement setup. (b) Enlarged view of the tilting bullet (b)

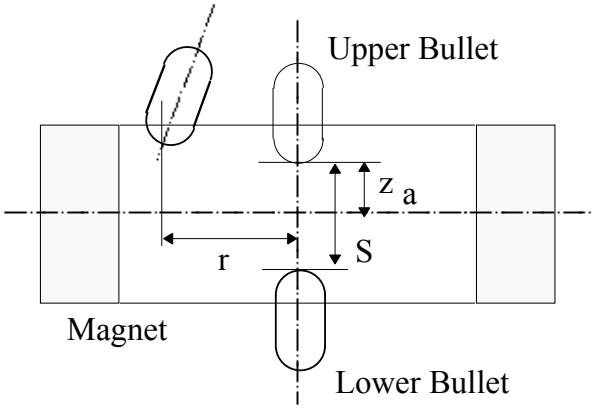

Fig. 5.9 Illustration of the radial force test of two bullets.

The radial displacement r was measured from the center, as shown in Fig. 5.9. Fig. 5.10 shows measured radial forces for two bullets. One of them (the lower bullet) was fixed on the magnet axis at z_a = 20 mm from the magnet center plain. The original separation between the bullets was S = 40 mm. The radial forces are plotted as a function of the

radial displacement r. Figs. 5.10 (a) and (b) are for the rounded rod and cylinder bullets, respectively. The radial forces were not significantly large, but once the bullet started moving away from the axis, then the radial forces increased.

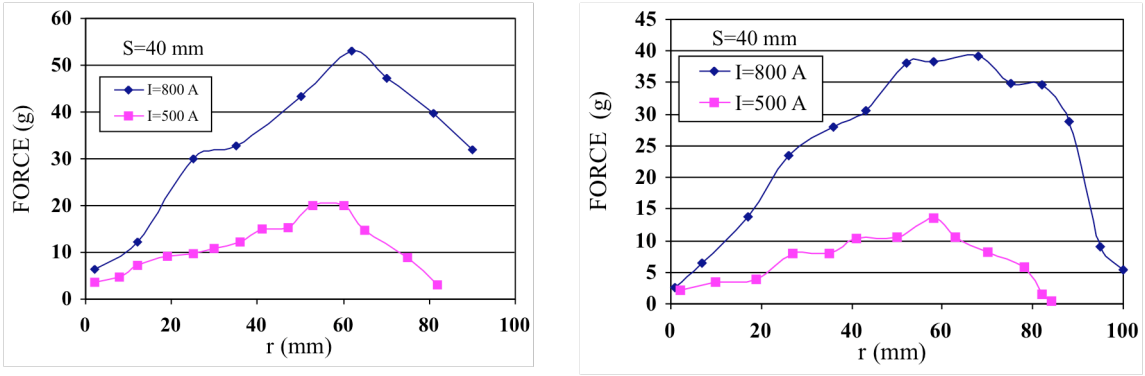

(a) (b)

Fig. 5.10 Measured radial force for two bullets where one of them was fixed on the magnet axis at 20 mm from the magnet center plain. The original separation between the bullets was 40 mm. The radial forces are plotted as a function of the radial displacement r. (a) Rounded rod bullet and (b) Cylinder bullet.

5.4.2 One-bullet radial force

Fig. 5.11 shows radial forces measured for one bullet with various starting location z_a measured from the magnet center (See Fig. 5.12). Both rounded rod and cylinder bullets showed very similar behaviors with regard to the distance z_a. If the bullet location was near the magnet center plane, the radial force increased with increasing the radial displacement r. When the distance z_a increases, the radial force show the maximum before reaching the magnet and the magnetic force decreases. If the bullet is moved away from the magnet (larger z_a), the radial force become smaller and decrease with increasing the radial displacement.

6. Magnetic Force and Field Analyses

6.1 Magnetic Force and Field Analysis Methods

The magnetic bullets are relative large compared with the magnet size, therefore the simple dipole theory is not applicable for our application. Calculation methods to analyze the magnetic force on the bullets and the magnetic fields have been developed. Basic concepts of the analytical method used is summarized:

1. The rounded rod bullet is approximated by a flat-end rod of the same volume having the same diameter.
2. The field value to magnetize a bullet is approximated by the middle field on the bullet.

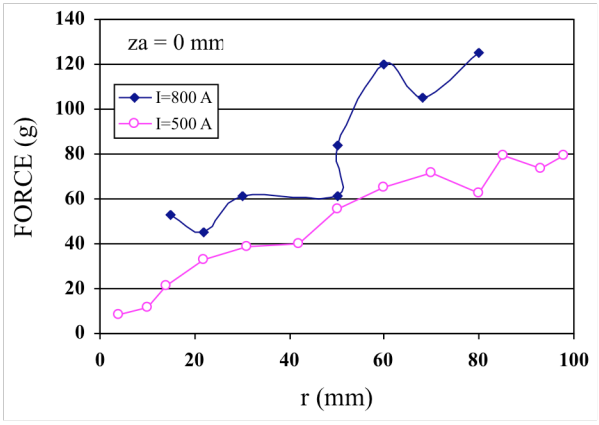

z_a = 0 mm

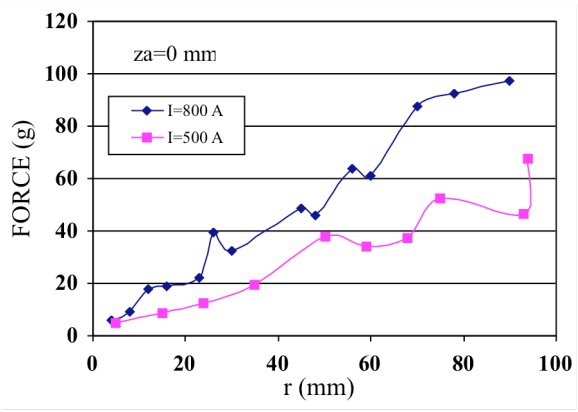

z_a = 0 mm

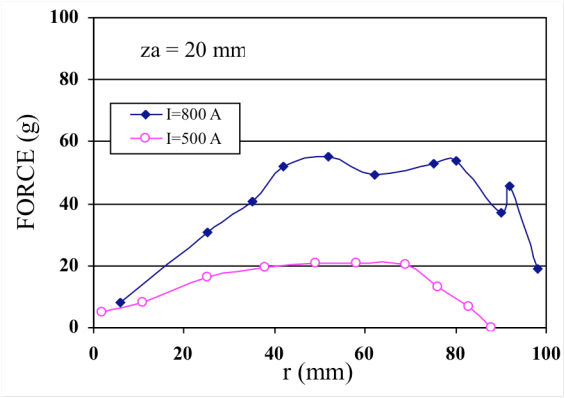

z_a = 20 mm

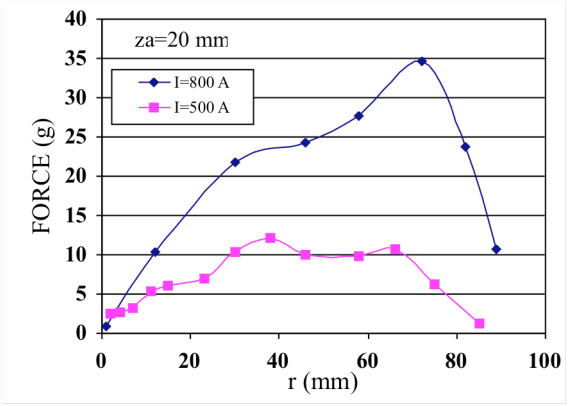

z_a = 20 mm

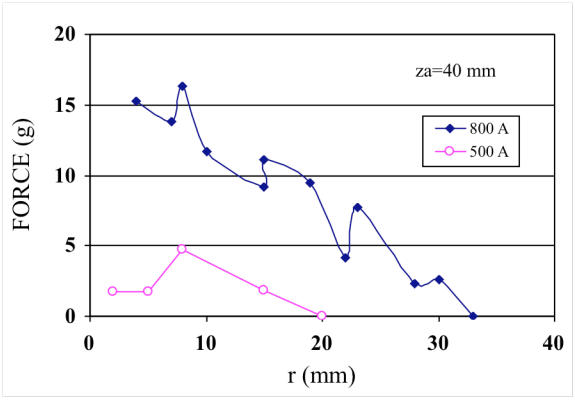

z_a = 40 mm

(a)

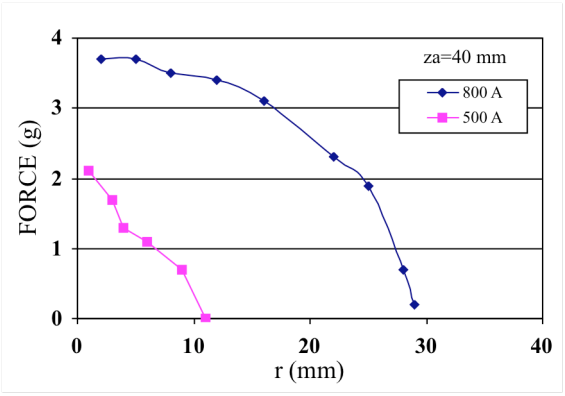

z_a = 40 mm

(b)

Fig. 5.11 Measured radial forces for one bullet with various starting locations z_a = 0, 20 mm and 40 mm as a function of the radial distance r. (a) Rounded rod bullet, (b) Cylinder bullet.

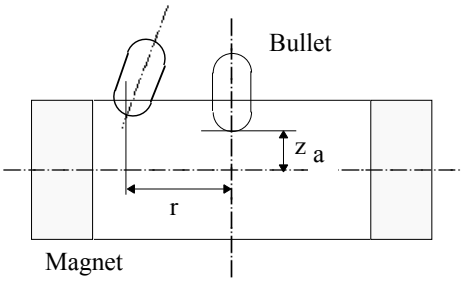

Fig. 5.12 Illustration of the radial force test of one bullet.

3. The bullet magnetization creates a magnetic field on the other bullet. For the rod bullet the induced field on the bullet axis is used. However, for the cylinder the field on the cylinder surface is used.
4. The field induced by the bullet magnetization gives a feedback to the magnet background field. The resulting field and magnetization are calculated by iteration.
5. Magnetic force on a bullet is obtained from the difference of the products of magnetization and Field (J_m x H) between the ends of the bullet. The magnetization for the force calculation is obtained from the averaged value between the end values and the mid-value of the bullet.
6. The field due to the magnetization of the rounded rod bullet is calculated using a smaller diameter rod model of the same length and the same volume. This method gave better fittings for short separation arrangements of the bullets.
7. All calculations were performed by Microsoft Excel®.

6.2 Analytical Force Equations

6.2.1 Rounded rod bullet

Cross-section of the rounded rod bullet shown in Fig. 4.1 is illustrated in Fig. 6.1. The actual dimensions were a=5 mm and L=25 mm. For force calculations, the rounded rod bullet was approximated by a rod having the same diameter and the same volume (Fig. 6.2), so that the approximated rod length is L-2a/3.

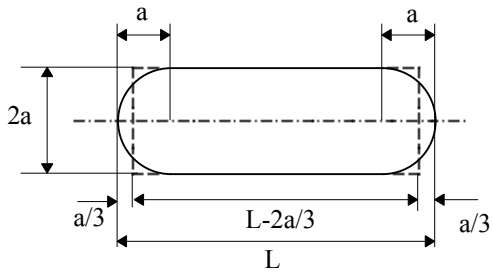

Fig. 6.1 Cross-section of the rounded rod bullet showing the dimensions

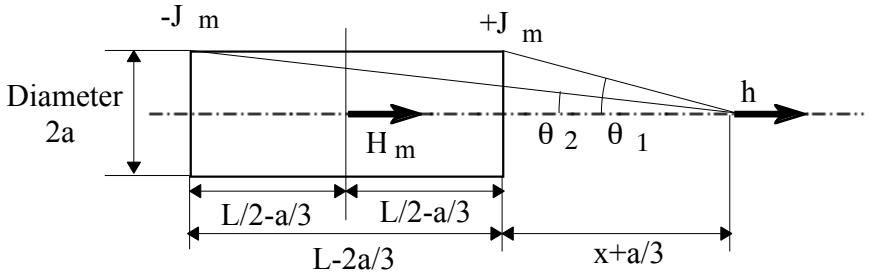

Fig. 6.2 Calculation model of the rounded rod bullet to analyze magnetization field.

The bullet is magnetized in a magnetic field. To calculate the magnetization J_m, the center field H_m is used, and J_m, is given as a function of the field H by Eq. 4.1.

The magnetized bullet creates magnetic field h at the distance x from the rounded rod bullet surface. The field h is given by the following equation [7];

$$h = \frac{J_m}{2\mu_0}\left(\cos\theta_2 - \cos\theta_1\right) \qquad (6.1)$$

where,

$$\cos\theta_1 = \frac{x + \frac{a}{3}}{\sqrt{\left(x + \frac{a}{3}\right)^2 + a^2}}$$

$$\cos\theta_2 = \frac{x + L - \frac{a}{3}}{\sqrt{\left(x + L - \frac{a}{3}\right)^2 + a^2}}$$

This magnetic field due to the magnetization J_m of the first bullet affects the magnetization of the second bullet. The magnetization of the second bullet induces an additional magnetic field affecting the first bullet. To solve this circulating effect the additional induced field is added to the background field. Then the force calculation was performed by iteration using Microsoft Excel®.

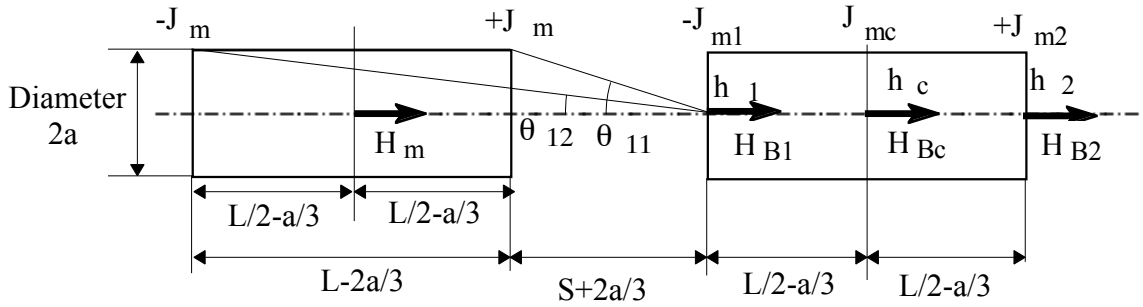

Fig. 6.3 Force analysis model for the round rod bullet.

The force analysis model for the two rod bullets is shown in Fig. 6.3. The resulting magnetic fields h_m with θ_{mn} (m=1, 2 and c, n=1 and 2) at the left end (m=1), the right end (m=2) and the center (m=c) of the second bullet, respectively, are given in the same way as Eq. 6.1;

$$
\begin{aligned}
h_1 &= \frac{J_m}{2\mu_0}\left(\cos\theta_{12} - \cos\theta_{11}\right) \\
h_2 &= \frac{J_m}{2\mu_0}\left(\cos\theta_{22} - \cos\theta_{21}\right) \\
h_c &= \frac{J_m}{2\mu_0}\left(\cos\theta_{c2} - \cos\theta_{c1}\right)
\end{aligned}
\qquad (6.2)
$$

Now the magnetic force F experienced by the rounded rod bullets is calculated with the summation of J_m x H over the bullet. The summation of the products can be approximated by an averaged magnetization with the center value J_{mc} and the edge value J_{m1} or J_{m2}. The bullet magnetic force is given by;

$$
F = \frac{1}{2\mu_0}\left\{\frac{J_{m1} + J_{mc}}{2}\cdot\left(h_1 + H_{B1}\right) - \frac{J_{m2} + J_{mc}}{2}\cdot\left(h_2 + H_{B2}\right)\right\} \qquad (6.3)
$$

where,

$$
\begin{aligned}
J_{m1} &= J_m\left(h_1 + H_{B1}\right) \\
J_{m2} &= J_m\left(h_2 + H_{B2}\right) \\
J_{mc} &= J_m\left(h_c + H_{Bc}\right)
\end{aligned}
$$

H_{B1}, H_{B2}, and H_{Bc} are the background field,

$$
\cos\theta_{11} = \frac{S + \frac{2a}{3}}{\sqrt{\left(S + \frac{2a}{3}\right)^2 + a^2}} \qquad \cos\theta_{12} = \frac{S + L}{\sqrt{(S + L)^2 + a^2}}
$$

$$\cos\theta_{21} = \frac{S+L}{\sqrt{(S+L)^2 + a^2}} \qquad \cos\theta_{22} = \frac{S+2L-\frac{2a}{3}}{\sqrt{\left(S+2L-\frac{2a}{3}\right)^2 + a^2}}$$

$$\cos\theta_{c1} = \frac{S+\frac{L}{2}+\frac{a}{3}}{\sqrt{\left(S+\frac{L}{2}+\frac{a}{3}\right)^2 + a^2}} \qquad \cos\theta_{c2} = \frac{S+\frac{3L}{2}-\frac{a}{3}}{\sqrt{\left(S+\frac{3L}{2}-\frac{a}{3}\right)^2 + a^2}}$$

Measured magnet-center fields for the bullet separation S < 15 mm did not agree well with the calculated values by the model showing in Fig. 6.1, even if the magnetic force agreed well each other. The length of the bullet in the model shown in Fig. 6.1 is about 3.3 mm shorter than the actual length, therefore calculated values seems not to agree with the measured values for the short range. An alternate model having the same length and the same volume, but smaller diameter, shown in Fig. 6.4, gave a better approximation for the fields. The field was calculated by Eq. 6.4.

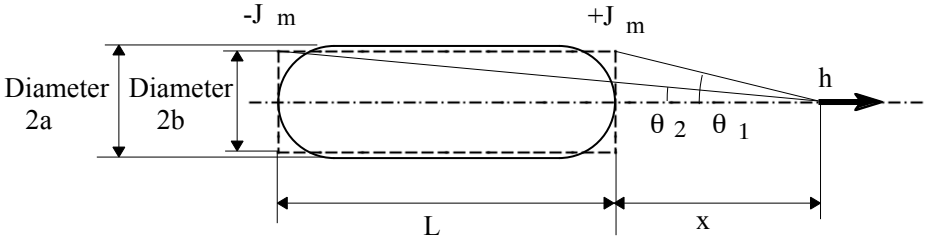

Fig. 6.4 Bullet model of the rod bullet for a short range magnetization field.

$$H = h + H_B \qquad (6.4)$$

here,

$$h = \frac{J_m}{2\mu_0}\left(\cos\theta_2 - \cos\theta_1\right)$$

$$\cos\theta_1 = \frac{x}{\sqrt{x^2 + b^2}} \qquad \cos\theta_2 = \frac{x+L}{\sqrt{(x+L)^2 + b^2}}$$

The above analyses of the force and field were for a pair of two bullets. However the field and force for one bullet can be calculated using the same equations without iteration since h = 0.

6.2.2 Hollow cylinder bullet

Cross-section of the cylinder bullet shown in Fig. 4.1 is illustrated in Fig. 6.5. The actual dimensions were a=5 mm, d=3.5 and L=25 mm.

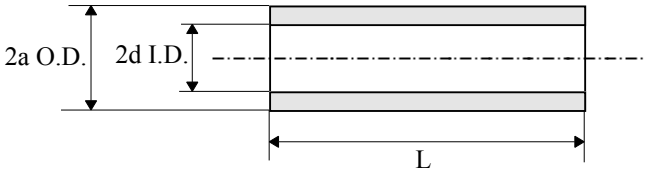

Fig. 6.5 Cross-section of the cylinder bullet showing the dimensions.

In the case of a hollow tube, the effective magnetic field to magnetize the tube could be approximated by the field h on the cylinder surface instead of the axial field h_a in Fig. 6.6.

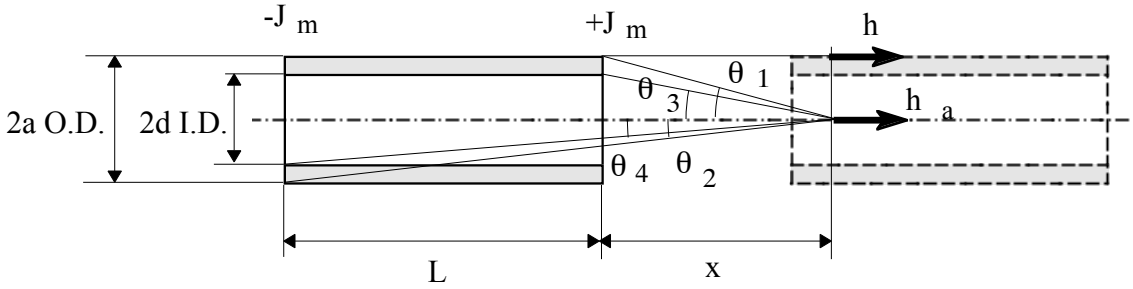

Fig. 6.6 Effective field analysis mode on the cylinder bullet.

The surface field h on the cylinder surface is written with the axial field h_a by

$$h = h_a \cdot \cos^2\theta \qquad (6.5)$$

Therefore the cylinder surface field h is obtained by

$$\begin{aligned} h &= \frac{-J_m}{2\mu_0}\int_{\theta_1}^{\theta_2} \sin\varphi \cdot \cos^2\varphi \cdot d\varphi - \frac{-J_m}{2\mu_0}\int_{\theta_3}^{\theta_4} \sin\varphi \cdot \cos^2\varphi \cdot d\varphi \\ &= \frac{J_m}{6\mu_0}\left(\cos^3\theta_2 - \cos^3\theta_1\right) - \frac{J_m}{6\mu_0}\left(\cos^3\theta_4 - \cos^3\theta_3\right) \end{aligned} \qquad (6.6)$$

Using Eq. (6.6), the magnetic force F acting on the cylinder bullets, illustrated in Fig. 6.7, is obtained in the similar method as that for the round rod bullets, and is given by Eq. (6.7).

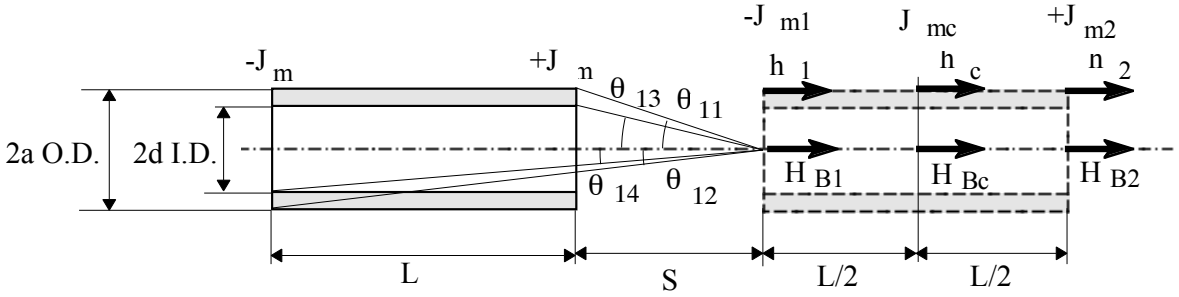

Fig. 6.7 Force analysis model for the cylinder bullet.

$$F = \frac{1}{2\mu_0}\left\{\frac{J_{m1}+J_{mc}}{2}\cdot\left(h_1+H_{B1}\right)+\frac{J_{m2}+J_{mc}}{2}\cdot\left(h_2+H_{B2}\right)\right\} \tag{6.7}$$

where,

$$J_{m1} = J_m\left(h_1+H_{B1}\right)$$
$$J_{m2} = J_m\left(h_2+H_{B2}\right)$$
$$J_{mc} = J_m\left(h_c+H_{Bc}\right)$$
$$h_1 = \frac{J_m}{6\mu_0}\left(\cos^3\theta_{12}-\cos^3\theta_{11}\right)-\frac{J_m}{6\mu_0}\left(\cos^3\theta_{14}-\cos^3\theta_{13}\right)$$
$$h_2 = \frac{J_m}{6\mu_0}\left(\cos^3\theta_{22}-\cos^3\theta_{21}\right)-\frac{J_m}{6\mu_0}\left(\cos^3\theta_{24}-\cos^3\theta_{23}\right)$$
$$h_c = \frac{J_m}{6\mu_0}\left(\cos^3\theta_{c2}-\cos^3\theta_{c1}\right)-\frac{J_m}{6\mu_0}\left(\cos^3\theta_{c4}-\cos^3\theta_{c3}\right)$$

$$\cos\theta_{11} = \frac{S}{\sqrt{S^2+a^2}} \qquad \cos\theta_{12} = \frac{S+L}{\sqrt{(S+L)^2+a^2}}$$
$$\cos\theta_{13} = \frac{S}{\sqrt{S^2+d^2}} \qquad \cos\theta_{14} = \frac{S+L}{\sqrt{(S+L)^2+d^2}}$$
$$\cos\theta_{21} = \frac{S+L}{\sqrt{(S+L)^2+a^2}} \qquad \cos\theta_{22} = \frac{S+2L}{\sqrt{(S+2L)^2+a^2}}$$
$$\cos\theta_{23} = \frac{S+L}{\sqrt{(S+L)^2+d^2}} \qquad \cos\theta_{24} = \frac{S+2L}{\sqrt{(S+2L)^2+d^2}}$$
$$\cos\theta_{c1} = \frac{S+\frac{L}{2}}{\sqrt{\left(S+\frac{L}{2}\right)^2+a^2}} \qquad \cos\theta_{c2} = \frac{S+\frac{3L}{2}}{\sqrt{\left(S+\frac{3L}{2}\right)^2+a^2}}$$
$$\cos\theta_{c3} = \frac{S+\frac{L}{2}}{\sqrt{\left(S+\frac{L}{2}\right)^2+d^2}} \qquad \cos\theta_{c4} = \frac{S+\frac{3L}{2}}{\sqrt{\left(S+\frac{3L}{2}\right)^2+d^2}}$$

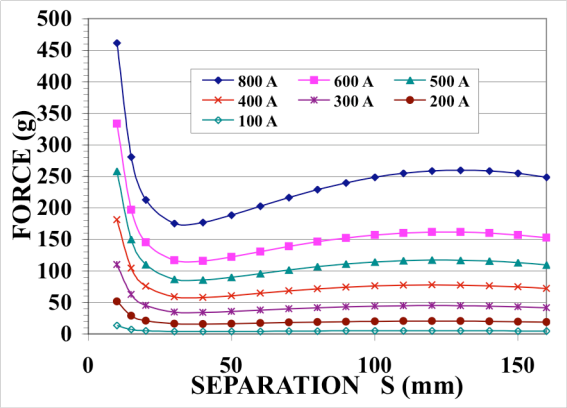

(a)

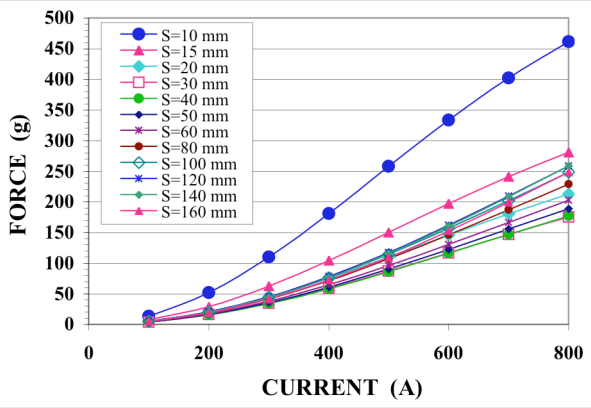

(b)

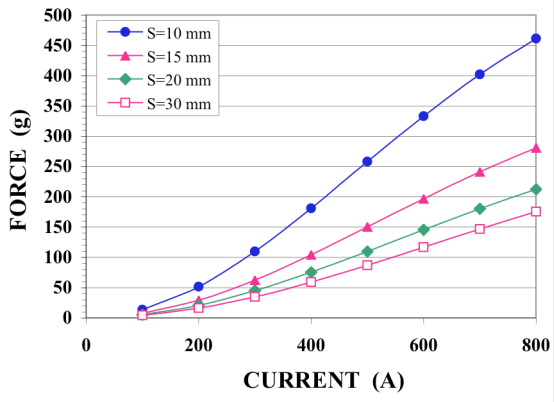

(c)

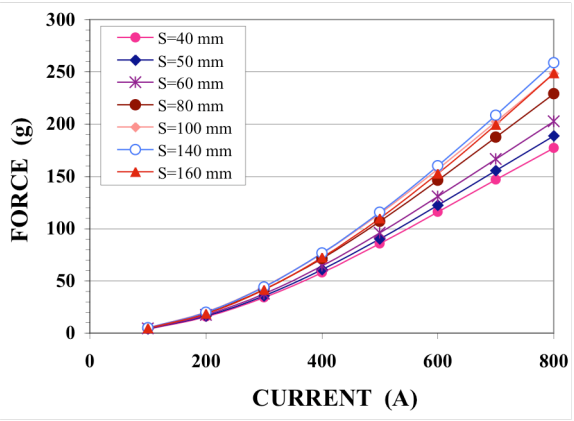

(d)

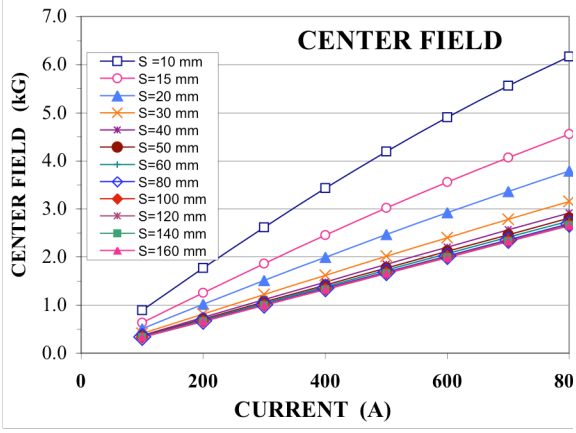

(e)

Rounded Rod Bullets
(25 mm length, 10 mm Diameter)

(f)

Fig. 6.8 Calculated Magnetic Force and center field for two rounded rod bullets.

6.3 Calculation Results

Magnetic forces and fields of two bullets of the rounded rod bullets and the cylinder bullets are analyzed with various separations between the bullets. One-bullet force and

off-centered two-bullet force are also analyzed. For these calculations the equations in the previous section were used with the magnet field of Eq. (3.7) and the magnetization equations of Eq. (4.1) for the rounded rod bullet and Eq. (4.2) for the cylinder bullet, respectively. Calculated results are compared with the measured results shown in the previous section.

6.3.1 Two Bullet Force

Rounded rod bullet

Fig. 6.8 shows calculated forces of the round rod bullet when two bullets are placed on the magnet axis symmetrically (the magnet center is at the center of two bullets.). The magnetic forces are plotted as a function of the separation distance between the bullets for various magnet currents in Fig. 6.8 (a). Figure (b) shows the force as a function of the current. These plots are separated into two figures (c) and (d) to show the details. The center field on the magnet axis is shown in Fig. 6.8 (e). As seen, these calculated results well agree with the experimental results shown in earlier.

Discrepancies between the calculation of Fig. 6.8 and the experimental results of Fig. 5.2 are shown in Table 6.1 and Fig. 6.9.

Table 6.1 Comparison between the calculation and experimental results for two-rounded-rod-bullet force.

Separation Between Bullets S (mm)	ERROR (%) (Calculated Force/Measured Force - 1) Current (A)						
	800	700	600	500	400	300	200
10	0.0	-2.9	-5.5	-2.2	6.3	15.0	31.0
15	0.8	-2.5	-4.9	-2.7	5.2	10.4	24.6
20	9.2	5.1	3.0	6.5	13.4	24.4	31.4
30	2.3	0.9	2.5	4.9	8.4	9.7	53.5
40	6.8	8.0	5.5	7.9	22.2	17.3	38.4
50	10.0	5.0	0.9	3.6	15.2	7.7	51.9
60	7.1	4.3	6.3	8.4	16.8	14.7	26.2
80	6.4	9.9	12.8	16.0	21.0	26.5	39.8
100	10.4	11.4	12.8	13.7	21.4	26.1	36.8
120	8.6	9.6	14.3	16.7	20.4	24.0	26.1
140	10.4	11.2	13.3	17.3	21.0	22.0	17.6
160	6.6	8.6	12.8	15.4	15.6	21.8	17.8

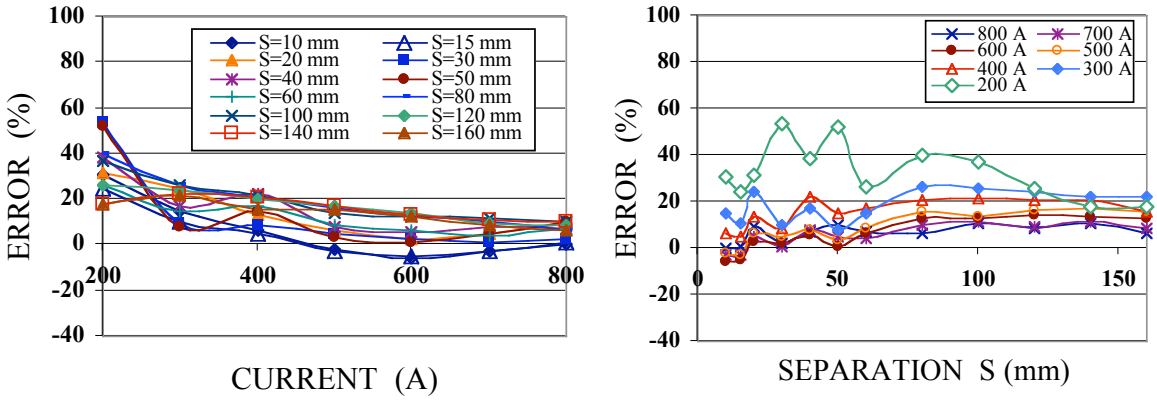

(a) (b)

Fig. 6.9 Comparison between the calculation and experimental results for two-rounded-rod-bullet force.

Hollow cylinder bullet

Fig. 6.10 shows similar plots to Fig. 6.8, but for the cylinder bullet. Discrepancies between the calculation of Fig. 6.10 and the experimental results of Fig. 5.3 are shown in Table 6.2 and Fig. 6.11.

Table 6.2 Comparison between the calculation and experimental results for two-cylinder-bullet force.

Separation Between Bullets S (mm)	ERROR (%) (Calculated Force/Measured Force - 1) Current (A)						
	800	700	600	500	400	300	200
10	-1.0	2.1	6.0	10.1	14.0	15.2	27.8
15	3.9	6.6	11.3	17.4	21.6	22.5	37.7
20	0.1	1.4	6.6	10.0	14.4	16.3	33.1
30	-7.3	-6.1	3.0	6.3	9.7	12.8	26.2
40	-6.0	-1.3	-0.4	3.0	5.0	7.2	36.3
50	-5.0	-0.8	-0.9	5.7	8.7	9.9	32.9
60	-6.4	-2.9	3.6	7.2	10.3	12.1	41.3
80	-4.1	-2.2	1.3	4.6	12.3	18.3	34.2
100	-1.8	-0.3	2.5	6.6	7.9	19.4	36.8
120	-0.6	4.1	7.8	10.1	11.0	19.1	36.1
140	1.6	3.5	5.8	8.7	9.9	20.8	29.6
160	1.1	2.9	6.0	7.5	10.5	18.9	35.6

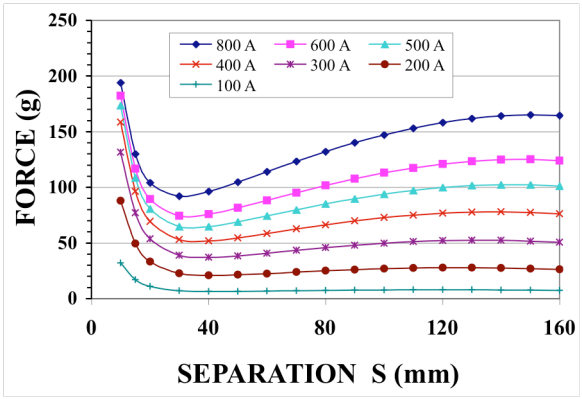

(a)

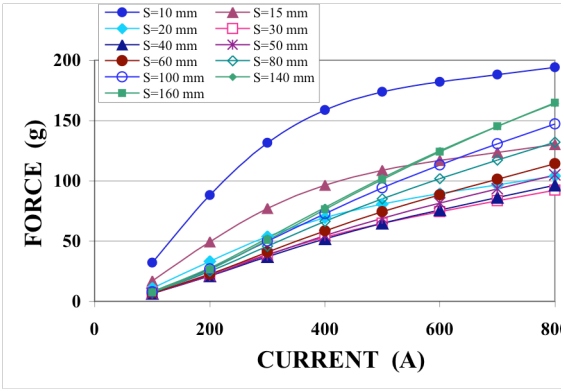

(b)

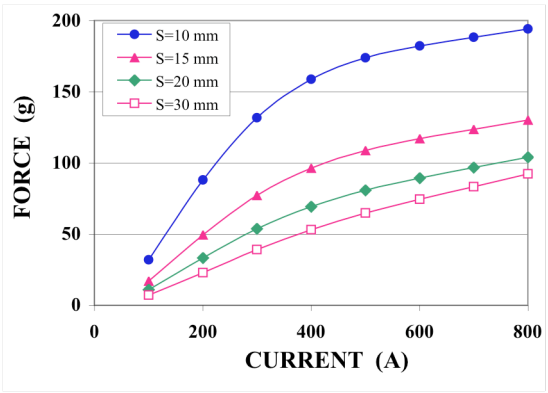

(c)

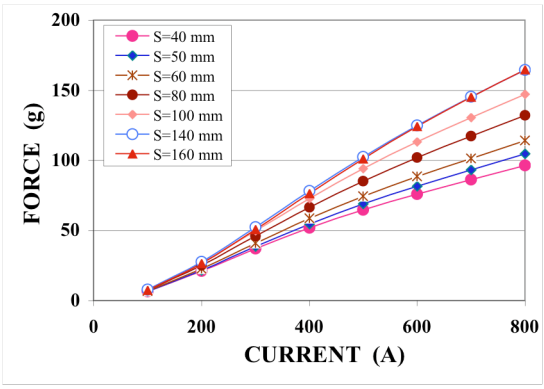

(d)

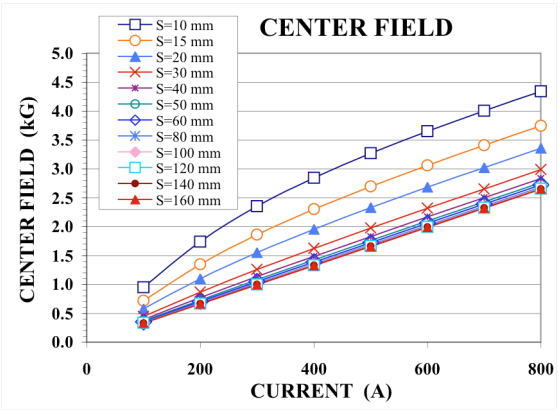

(e)

Hollow Cylinder Bullets
(25 mm length, 10 mm OD, 7 mm ID)

(f)

Fig. 6.10 Calculated Magnetic Force and center field for two Cylinder Bullets.

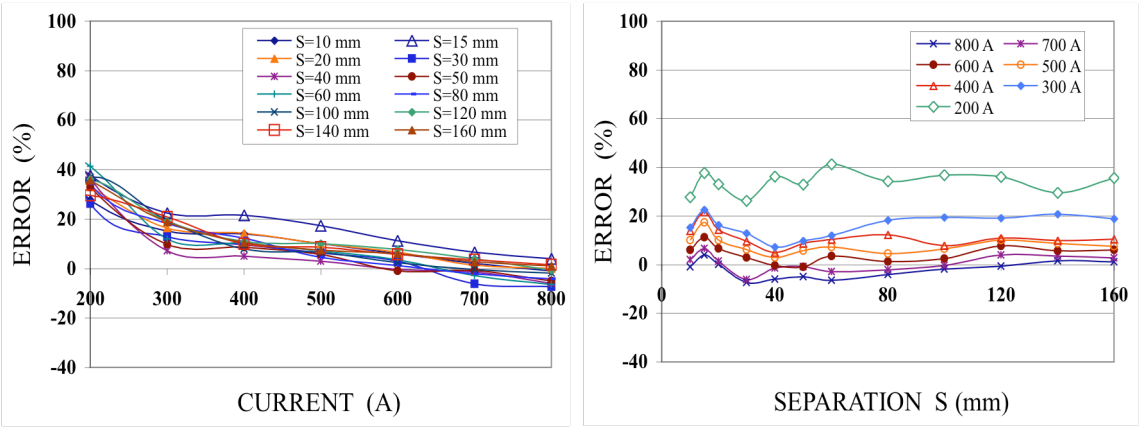

(a) (b)

Fig. 6.11 Comparison between the calculation and experimental results for two-cylinder-bullet force.

6.3.2 One Bullet Force

Rounded rod bullet

Forces on one rounded rod bullet on the magnet axis are calculated. The results are shown in Fig. 6.12. The distance z_a is from the magnet center to the bullet.

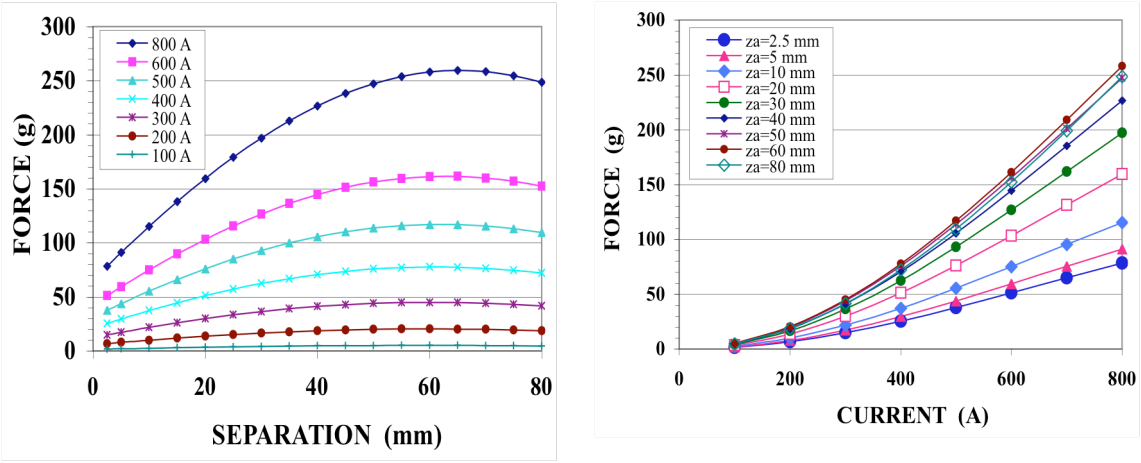

(a) (b)

Fig. 6.12 Calculated Magnetic Force for one rounded rod bullet.

Discrepancies between the calculation of Fig. 6.12 and the experimental results of Fig. 5.5 (a) are shown in Table 6.3 and Fig. 6.13.

Table 6.3 Comparison between the calculation and experimental results for one-rounded-rod-bullet force.

Separation Between Bullets S (mm)	ERROR (%) (Calculated Force/Measured Force - 1) Current (A)						
	800	700	600	500	400	300	200
2.5	7.7	11.4	10.3	3.2	14.7	15.4	7.3
5	14.9	8.3	1.8	7.7	6.4	120.2	171.4
10	6.0	9.7	14.4	12.5	32.3	69.6	54.1
15	15.8	13.9	12.6	17.4	25.2	43.9	59.3
20	13.2	11.7	13.3	21.8	22.7	55.6	32.0
30	14.7	12.7	15.2	19.9	23.4	32.8	37.8
40	12.6	11.8	13.2	17.4	22.4	29.8	39.7
50	10.2	9.9	12.5	17.4	22.2	26.0	33.9
60	8.7	9.8	13.2	18.8	23.0	31.0	29.6
80	5.8	8.9	13.8	17.8	19.4	16.4	15.1

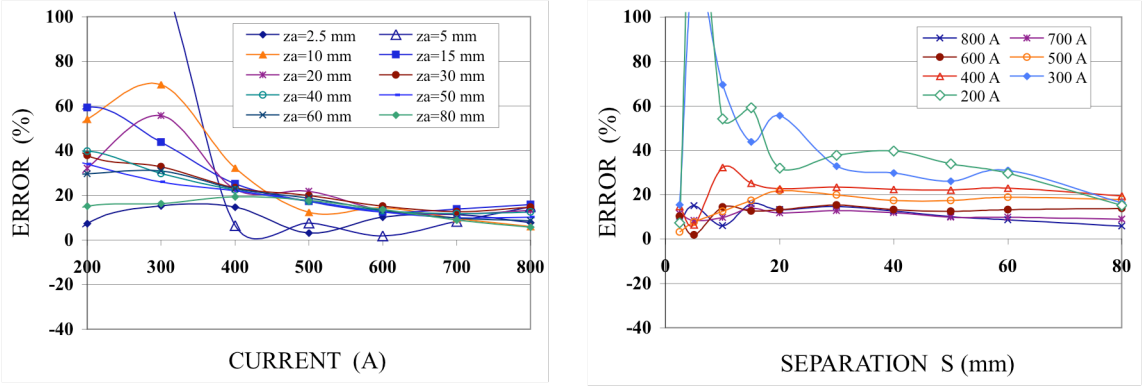

(a) (b)

Fig. 6.13 Comparison between the calculation and experimental results for one-rounded-rod-bullet force.

Hollow cylinder bullet

Fig. 6.13 is similar to the previous figure, but for one cylinder. Discrepancies between the calculation of Fig. 6.14 and the experimental results of Fig. 5.5 (b) are shown in Table 6.4 and Fig. 6.15.

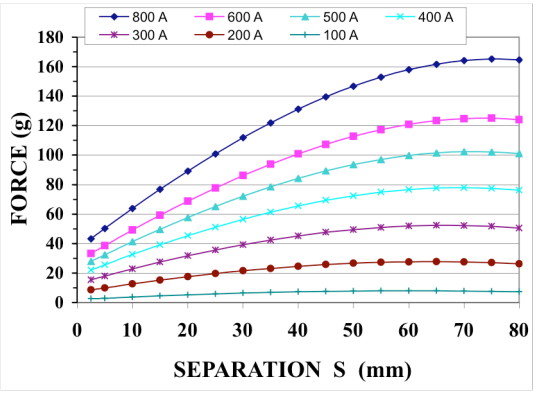

(a)

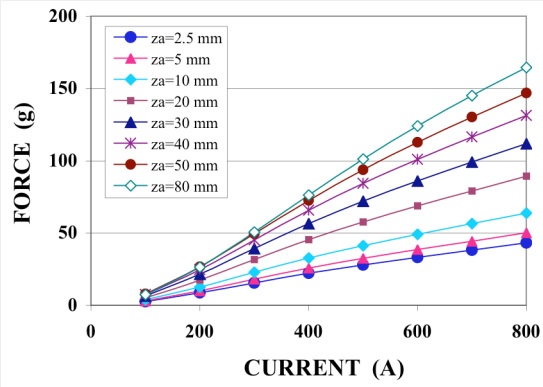

(b)

Fig. 6.14 Calculated Magnetic Force for one cylinder bullet.

Table 6.4 Comparison between the calculation and experimental results for one-cylinder-bullet force.

Separation Between Bullets S (mm)	ERROR (%) (Calculated Force/Measured Force - 1) Current (A)						
	800	700	600	500	400	300	200
2.5	-3.2	-2.2	2.4	1.8	-2.3	1.1	10.5
5	-14.4	-10.9	-7.5	2.8	4.9	11.3	9.1
10	-3.3	-1.0	1.9	9.1	12.0	27.7	57.1
15	-8.9	-5.8	-3.4	0.7	9.4	13.0	45.3
20	-8.4	-5.5	-4.6	-0.1	4.0	7.6	31.7
30	-5.0	-1.6	2.2	6.5	9.9	19.7	38.1
40	-4.1	-1.8	2.3	7.7	9.7	17.2	32.4
50	-4.2	-0.9	2.1	6.0	10.7	17.8	48.7
60	-3.0	-0.7	3.3	7.0	11.3	19.4	42.8
80	-3.2	-0.6	1.8	2.3	7.4	17.7	36.1

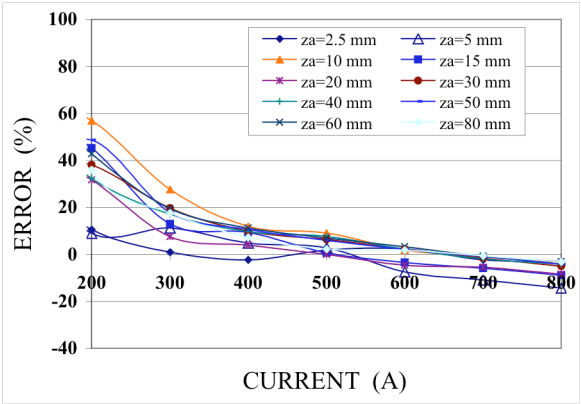

(a)

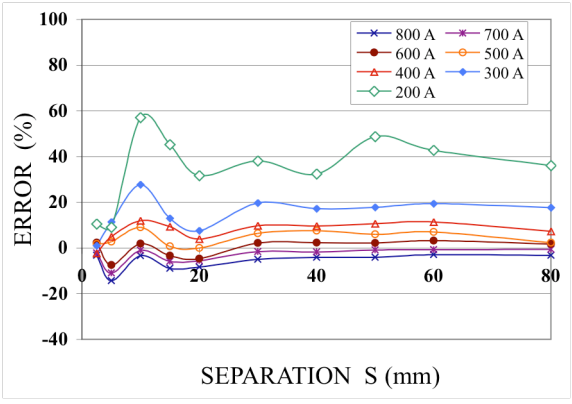

(b)

Fig. 6.15 Comparison between the calculation and experimental results for one-cylinder-bullet force.

6.3.3 Off-Centered Two-Bullet Force

Rounder rod bullet

If the center between two bullets is not at the center of the magnet, each bullet has a different magnetic. Magnetic forces of one rounded rod bullet (the upper bullet) of the two bullets are calculated with keeping the separation distance of 40 mm. The results are shown in Fig. 6.16 (a), (b) and (c). Figure (d) shows the force of the other bullet (the lower bullet).

Discrepancies between the calculation of Fig. 6.16 and the experimental results of Fig. 5.7 (a) are shown in Table 6.5 and Fig. 6.17.

Table 6.5 Comparison between the calculation and experimental results for two off-centered rounded rod bullet force.

Separation Between Bullets S (mm)	ERROR (%) (Calculated Force/Measured Force - 1) Current (A)						
	800	700	600	500	400	300	200
0	8.5	2.5	-1.8	11.3	-1.3	-9.7	-18.2
10	11.0	8.0	6.6	9.8	12.6	19.3	45.6
20	6.8	8.0	5.5	7.9	22.2	17.3	38.4
30	8.8	9.2	9.7	15.0	23.3	32.5	33.9
40	8.6	7.3	8.8	12.9	19.1	24.6	29.8

Hollow cylinder bullet

Fig. 6.17 shows the similar calculation results, but for the cylinder. Discrepancies between the calculation of Fig. 6.18 and the experimental results of Fig. 5.7 (b) are shown in Table 6.6 and Fig. 6.19.

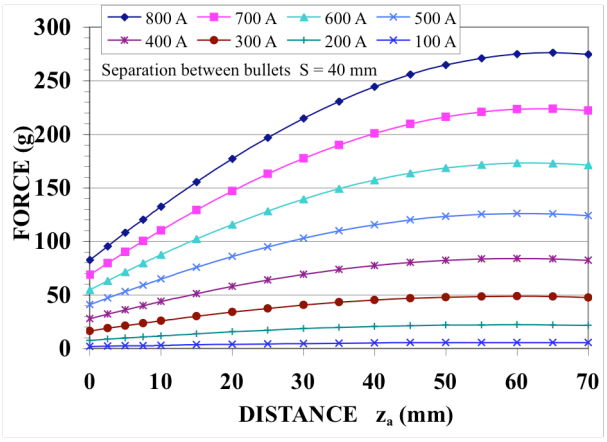

(a)

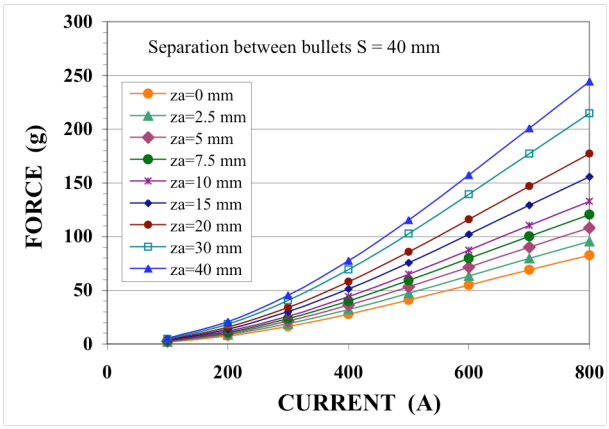

(b)

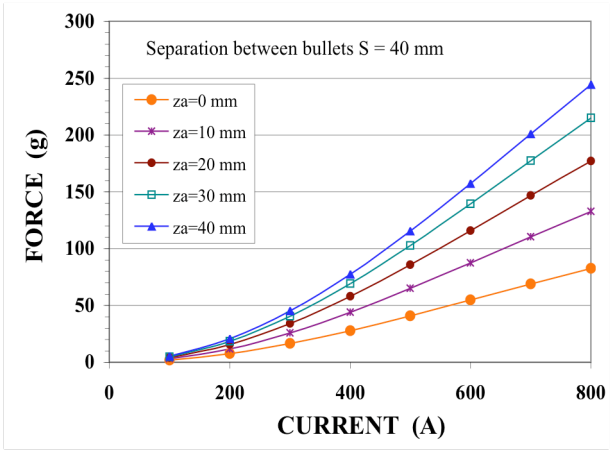

(c)

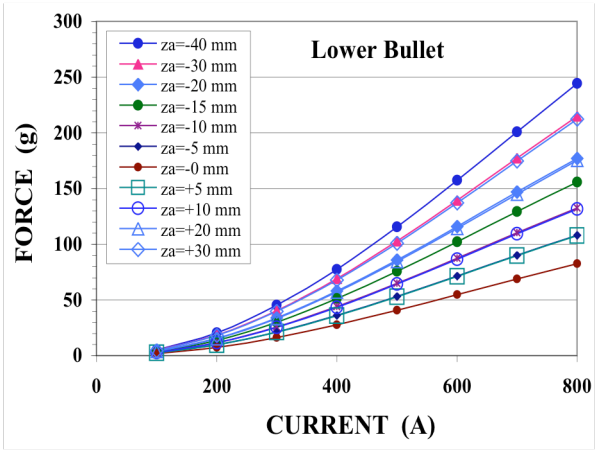

(d)

Fig. 6.16 Calculated Magnetic Force for two off-centered rounded rod bullets. The separation between two bullets is 40 mm. (a) – (c) For the upper bullet. (d) For the other lower bullet.

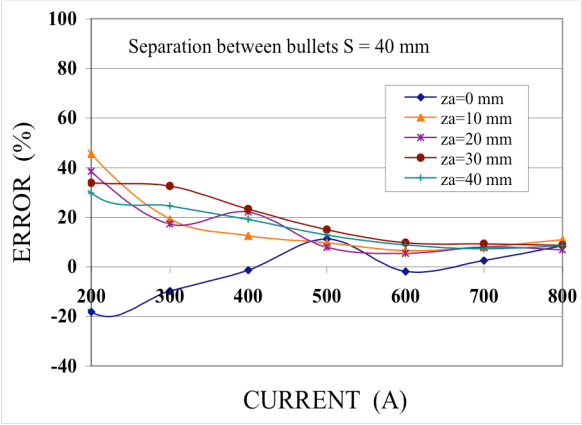

(a)

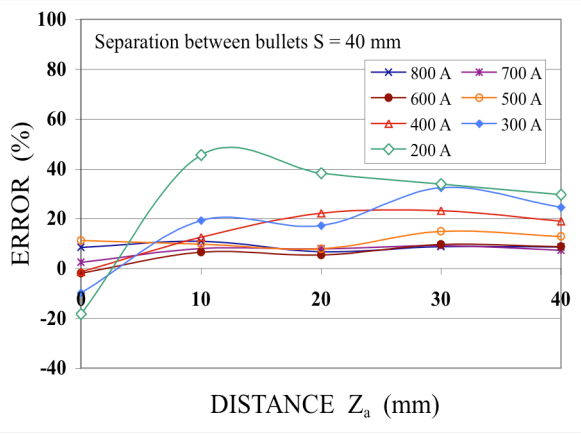

(b)

Fig. 6.17 Comparison between the calculation and experimental results for two off-centered rounded rod bullet force.

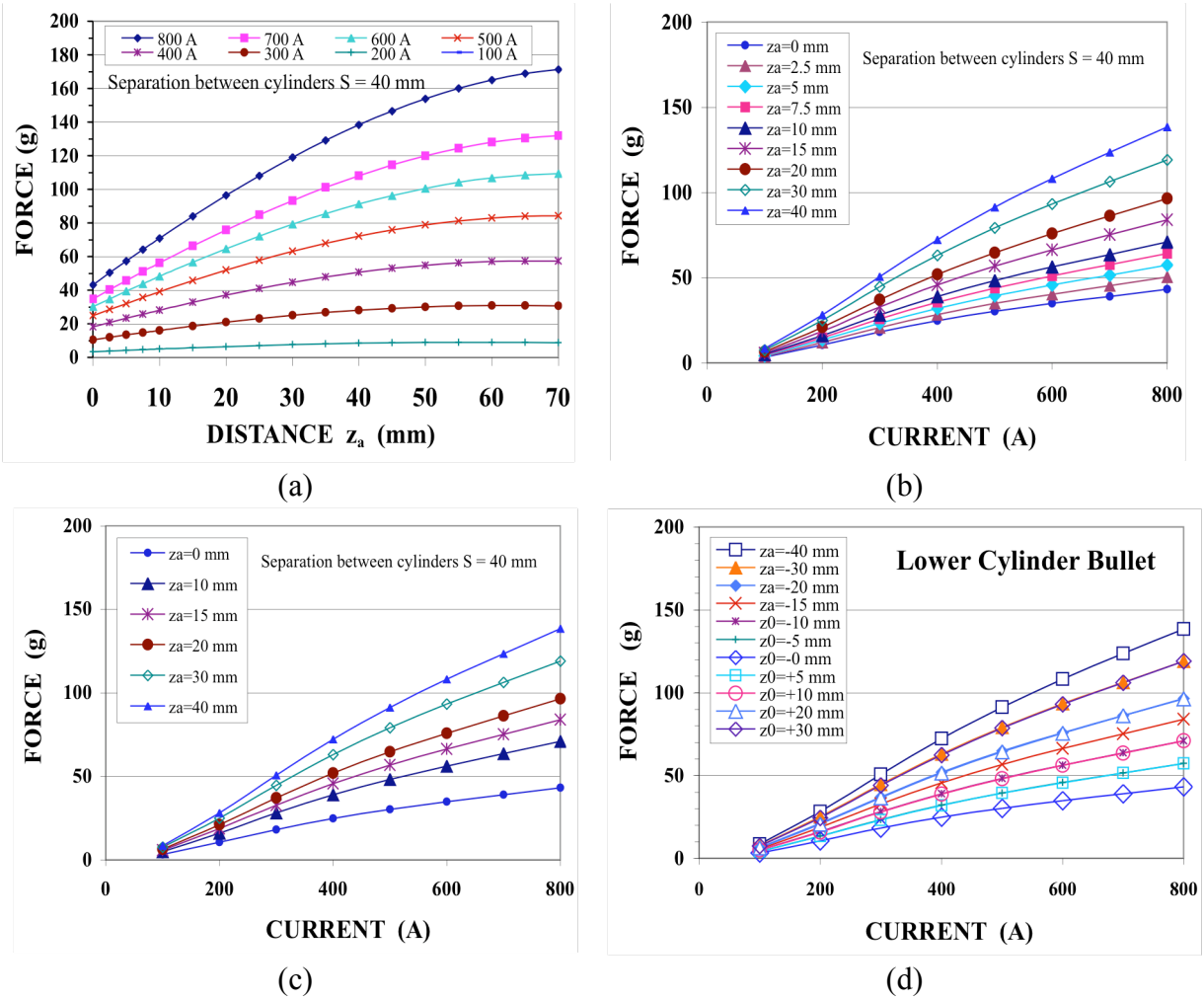

Fig. 6.18 Calculated Magnetic Force for two off-centered cylinder bullets. The separation between two bullets is 40 mm. (a) – (c) For the upper bullet. (d) For the other lower bullet.

Table 6.6 Comparison between the calculation and experimental results for two off-centered cylinder-bullet force.

Separation Between Bullets S (mm)	ERROR (%) (Calculated Force/Measured Force - 1) Current (A) 800	700	600	500	400	300	200
0	-14.5	-15.3	10.7	5.8	15.7	11.3	34.7
10	-14.0	-12.7	-10.3	1.9	5.8	7.7	31.0
20	-0.6	1.9	5.1	8.8	10.7	15.9	35.4
30	-3.9	-1.7	-0.8	3.3	4.0	15.3	21.0
40	-1.9	0.7	3.2	8.8	11.8	17.2	37.0

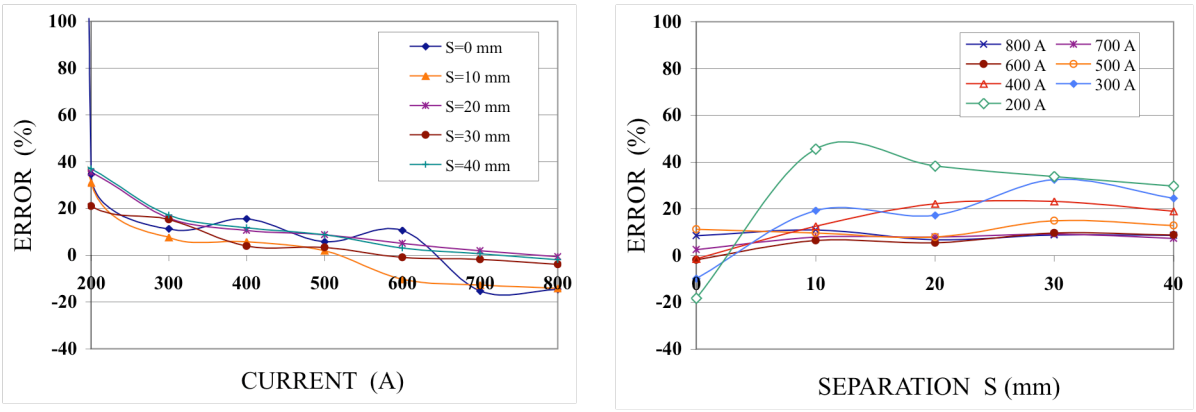

(a) (b)

Fig. 6.19 Comparison between the calculation and experimental results for two off-entered cylinder-bullet force.

7. Pressure Monitoring Method

In order to monitor the pressure of the bullet acting on tissue during the treatments, a wire less capsule type device will be used. A wireless pressure device "SmartPill" is commercially available from SmartPill Co. The capsule is illustrated below [8]. It has been developed to aid in the diagnosis of motility disorders, Gastroparesis and Dyspepsia by accurately measuring internal pressure and pH in a human body.

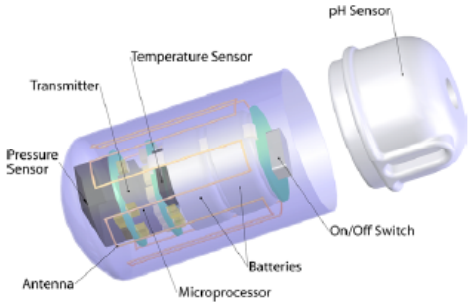

Fig. 7.1 SmartPill ACT-I capsule from
http://www.smartpilldiagnostics.com/news_kit.php.

The SmartPill capsule is 27 mm long x 11.7 mm diameter, containing pressure, pH and temperature sensors. Data obtained by these sensors are transmitted to SmartPill Data Receiver near by the patient. The data stored in the receiver is facilitated by SmartPill PC Software. The pressure sensor working range is 0 – 250 mmHg (about 340 g). More detail information is available at www.smartpillcorp.com. The capsule might be easily adapted to our magnetic bullet with minor modifications. Battery lifetime is expected to be about 72 hours. However, the battery could be switched on and off remotely by a minor modification.

SmartPill was tested using our force measurement setup. Tested SmartPill was obtained from the company with the data receiving devices shown in Fig. 7.2. The SmartPill was mounted on the load cell using a plastic tube, as shown in Fig. 7.3. The SmatPill capsule mounted at the bottom of the tube and the rod bullet were placed above SmartPill (see Fig. 3.3 (b)), so that the magnetic force pressures on SmartPill. The pressure detected by SmartPill was transmitted to the SmartPill receiver. Unfortunately the communication was interrupted when the magnetic field increased. The remote reed switch was suspected to interfere with the magnetic field and stop the operation. It will be improved for this application if necessary.

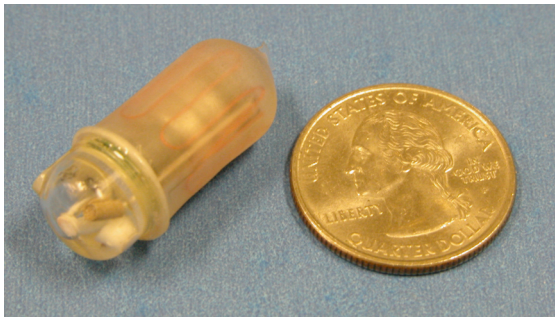

(a)

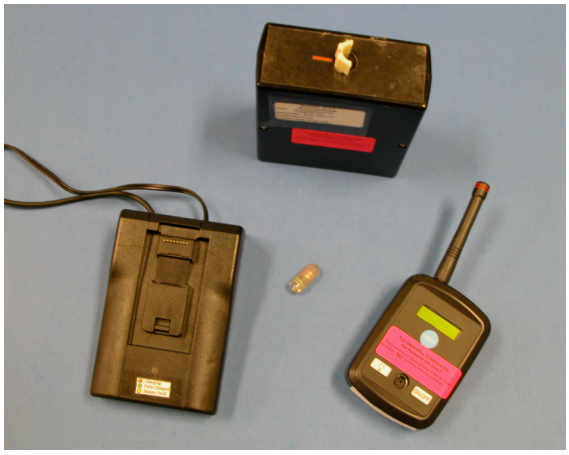

(b)

Fig. 7.2 (a) SmartPill capsule with a Quarter coin. (b) Receiver (right), receiver docking station (left) and switch controller (top) with SmartPill at the center.

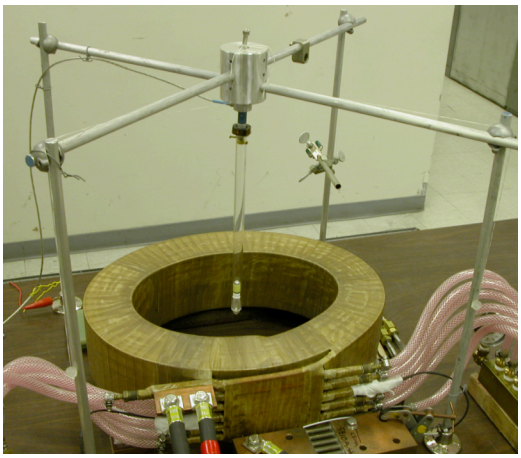

(a)

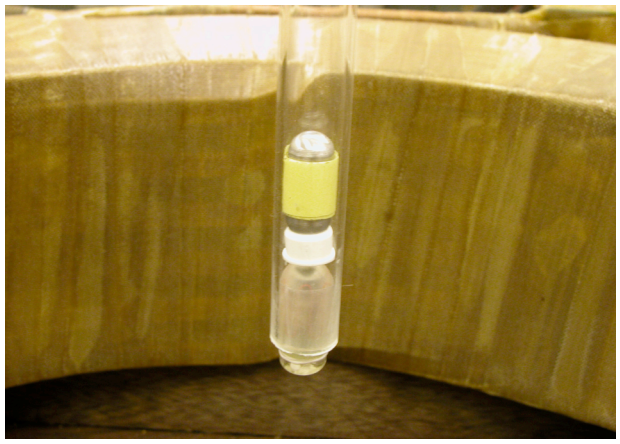

(b)

Fig. 7.3 (a) SmartPill test setup. (b) Enlarge setup of SmartPill mounting in a tube. Bullet is placed on SmartPill to be pressured by the bullet in a magnetic field.

8. Summary

Two types of bullets, solid rounded rod bullet and hollow cylinder bullet for an electromagnetic bougienage were developed and characterized using a fabricated

prototype bougienage magnet. A cylinder bullet has smaller demagnetization effect than a solid rod bullet. A cylinder type bullet can be magnetized effectively and creates a larger magnetic force even at low field than the solid rod bullet. The magnetic force increases with the volume, therefore a solid bullet can be smaller in size. The length of a bullet is also very effective factor to increase the magnetic force. Magnetic bullets should be designed and optimized to meet each application requirement. Analytical methods to obtain the magnetic forces acting on bougienage bullets were also discussed. The calculation results were confirmed to agree with the experimental results. The analytical equations obtained can be used for an active bougienage force control system while in use during hospital operation.

The results are as follows:

1. The magnet was confirmed to operate at the design current of 800 A (26 V, 20.7 kW). The electric resistance and inductance of the magnet are 32.3 m-Ohm and 2.73 mH, respectively. The center field of the magnet was 2.72 k-Oe at 800 A.
2. When the magnet is cooled with coolant flow of 2.2 gallons per minute, the temperature increase ΔT °C is given by $\Delta T = 5.6960 \cdot 10^{-5} \cdot I^2$ (I is the current in ampere.).
3. Calculated field H in Oe is written on the magnet axis as a function of the distance x in mm ($x < 80$ mm) from the magnet center and the current I in ampere;
   $H = (2.0885\text{x}10^{-9}\ x^4 + 1.8797\text{x}10^{-7}\ x^3 - 1.4406\text{x}10^{-4}\ x^2 + 6.4422\text{x}10^{-5}\ x + 3.3060)\ I$
   The calculated field was 2.72% smaller than the measured value.
4. Two types of bougie bullets, rounded rod and hollow cylinder bullets, were developed. Their measured magnetization vs. field curves were given by approximated equations as follows:
   Rounded rod bullet:

$$J_m(H) = -2.3986\ 10^{-19} H^5 + 5.270810^{-15} H^4 - 3.5226\ 10^{-11} H^3 + 1.474610^{-8} H^2 + 6.3306\ 10^{-4} H + 2.7062\ 10^{-3}$$

   Hollow cylinder bullet:

$$J_m(H) = -1.4105\ 10^{-22} H^6 + 4.4854\ 10^{-18} H^5 - 5.7173\ 10^{-14} H^4 + 3.7226\ 10^{-10} H^3 - 1.3024\ 10^{-6} H^2 + 2.3417\ 10^{-3} H - 9.1580\ 10^{-2}$$

   These equations were used for the force analysis.
5. Magnetic forces of the bullets were experimentally measured in detail.
6. When the separation between two bullets is less than about 30 mm, the magnetic forces of the bullets is enhanced by the magnetic mutual interference from each other. As the separation increases, the magnetic force is dominated more by the field gradient of the magnet than the mutual interference effect. Therefore, enough magnetic force can be created even one bullet.
7. Analytical methods to obtain the magnetic forces acting on bougienage bullets were developed. The calculation results were confirmed to agree with the experimental results. The errors of the calculations against the measurements for both cases of

two round rod bullets and two hollow cylinder bullets were below 8% for 400 A < I <800 A and S < 80 mm. The errors increase when the magnet currents are lower than 400 A.

8. Under a certain condition, bullets have radial forces as well as the axial force, and move toward the magnet winding. The radial forces were measured.
9. A wireless capsule type pressure sensor which is commercially available from SmartPill Co. was tested in a magnetic field. It was noted wireless capsule required a modification to use for our application in magnetic field.
10. Two types of bullets; solid rod (rounder rod bullet) and tube (hollow cylinder bullet) have been test as typical bougie bullets. A cylinder bullet has smaller demagnetization effect than a solid rod bullet, therefore a cylinder type bullet is magnetized effectively and creates a large magnetic force even at low field. The magnetic force increases with the volume, therefore a solid bullet can be smaller in size. The length of a bullet also very effective factor to improves the magnetic force. Magnetic bullet should be designed and optimized to meet each application requirements.
11. Bullets have the radial force as well as the axial force in the magnet. The radial force is not large near the magnet axis. In a certain condition the radial force might bother to obtain proper magnetic forces. It will be minimize the radial force by optimizing the magnet diameter and the thickness, or by a special design of the magnet winding shape.

Diagnostics development of the total system is in progress. The initial work at Children's Hospital will be undertaken as experimental surgery. A part of this work was presented at MT-20, Philadelphia, August 2007 [9].

Acknowledgements

The authors are grateful to Robert J. Weggel for designing the magnet and for useful discussions, and also to Luisa Chiesa for assistance with the measurements. The authors would like to thank Dr. John R. Semler, SmartPill Co. for providing SmartPill devices. This work was supported by the U.S. National Institute of Health and Children's Hospital Charitable Funds, Boston.

References

[1] Howard, R., Mayer, NA: Esophageal atresia: A technique for elongating the upper pouch. Surgery 58:725, 1965.
[2] Hendren, W.H. and Hale, J.R.: Lengthening of Esophageal Segments in Congenital Esophageal Atresia by Electromagnetic Bougienage. New Engl. J. Med 293:428, 1975.
[3] Hendren, W.H. and Hale, J.R.: Esophageal Atresia Treated by Electromagnetic Bougienage and Subsequent Repair. J. Pediatr. Surg. 11:723, 1976

[4] Hendren, W.H. and Hale, J.R.: High-Pouch Imperforate Anus Treated by Electromagnetic Bougienage and Subsequent Perineal Repair. J. Pediatr. Surg. 11:723, 1976.
[5] Zaritsky M, Ben R, Hauri J, Pelusso H, Ferrari C, Bertolotti J: Use of Magnets in the Primary Repair of the Esophageal Atresia, Meeting of the Argentine Congress of Radiology, October, 2003.
[6] Heinz E. Knoepfel, *Magnetic Fields*, John Wiley & Sons, Inc., 2000, p.92.
[7] ibid. p. 98.
[8] SmartPill website, http://www.smartpilldiagnostics.com/news_kit.php.
[9] M. Takayasu, D.B. Montgomery, and J.V. Minervini, "Characterization of Bougienage Electromagnetic Forces," IEEE Trans. Appl. Superconduct, 18, No. 2, 891-895, 2008.